Response to Reviewers

Manuscript egusphere-2026-4450

Highly oxygenated organic molecule formation from 2,5-dimethylfuran oxidation by O_3 and OH: an experimental and computational study

Reviewer comments • **Our responses** • **Changes to the manuscript**

We thank the reviewers for going through our manuscript titled 'Highly oxygenated organic molecule formation from 2,5-dimethylfuran oxidation by O_3 and OH: an experimental and computational study' and for their constructive suggestions on how to improve the work. We have incorporated all the suggestions and have modified the revised manuscript accordingly. Below, the reviewer queries are reproduced verbatim in red, followed by detailed point-by-point responses in purple, and the changes and additions to the revised manuscript in blue.

Referee #1

REVIEWER COMMENT R1.1

The discussion of the symmetry factor in Eq. (1) is either too short or some errors were made. The symmetry factor should account for ratios of rotational symmetry numbers and numbers of enantiomers. For the reaction of 2,5-DMF with O_3, the appropriate product and ratio of all the components (i.e., what the authors describe as the symmetry factor) should be eight, which correlates with the 8 ways that O_3 can add (from above or below the DMF plane, to the left of right double bond of DMF, and with either of two O_3 orientations). This 8 comes from 2 for the symmetry of DMF, 2 for the symmetry of O_3 and 2 for the number of enantiomers in the TS. For the reaction with OH, the ratio should instead by 4.

RESPONSE

We thank the reviewer for pointing this out. Following the reviewer's comment, we revisited the treatment of the symmetry factor and followed the discussion by Fernández-Ramos et al. (2007). The symmetry factors were corrected to 8 and 4 for the reactions of 2,5-DMF with O_3 and OH, respectively, accounting for the rotational symmetry numbers and mirror-image transition-state configurations.

CHANGES TO MANUSCRIPT

Methods section, lines 149–152: "The symmetry factor (σ) was set to 8, accounting for rotational symmetry numbers of 2 for 2,5-DMF and 2 for O_3, together with a factor of 2 from the two enantiomeric transition-state configurations (Fernández-Ramos et al., 2007). Similarly, for the OH-initiated reaction, σ was set to 4, accounting for the rotational symmetry number of 2 for 2,5-DMF and a factor of 2 from the two enantiomeric transition-state configurations."

REVIEWER COMMENT R1.2

It is hard to understand why LC-TST was used for the bimolecular reactions, while MC-TST was

used for the unimolecular reactions. Some rationale should be provided for these different choices in methodology.

RESPONSE

We agree with the reviewer that the rationale for using different TST treatments was not sufficiently explained in the original manuscript. The original choice between LC-TST and MC-TST was based on the conformational complexity of the species involved rather than on whether the reaction was bimolecular or unimolecular. For the bimolecular reactions of 2,5-DMF with O_3 and OH, both the reactants and the corresponding transition states have only one relevant conformer. Therefore, LC-TST was employed for these reactions. In contrast, the subsequent unimolecular pathways involved multiple energetically relevant conformers of the reactants and/or transition states, and MC-TST was therefore used to account for their individual contributions. We have now added this rationale to the Computational Methods section of the revised manuscript.

CHANGES TO MANUSCRIPT

Computational Methods section, lines 140–143: "Rate coefficients (k), defined by Eq. (1), for the bimolecular reactions of 2,5-DMF with O_3, OH addition to 2,5-DMF, and OH-initiated H-abstraction were calculated using lowest-conformer transition state theory (LC-TST), in which only the lowest-energy conformers of both the reactants and the corresponding transition states were considered. This approach was used because both the reactants and the corresponding transition states have only one relevant conformer."

REVIEWER COMMENT R1.3

The discussion of the T1 diagnostic, which presumably is meant to inform the reader regarding the appropriateness and accuracy of the calculations, could benefit from significant additional details. For example, it is well known that O3 itself is a highly multireference species. Similarly, CIs are well known to have substantive multireference character. In the latter case, it is clear from many literature studies that CCSD(T) based evaluations of CI energies are generally in error by about 1 kcal/mol. Diradical pathways can also be significant in the decomposition of a POZ. If these pathways had been treated, they would have even larger multireference effects.

One of the challenges for readers who are not experts in theory is in understanding the expected accuracy of theoretical calculations. Without this understanding it is very hard to understand the utility and/or limitations of the theoretical analysis. For this reason, it would be incredibly valuable to the general audience to provide some indication of the expected accuracy of the present calculations. While this is not yet the publication norm, I believe it should be. From my experience, I would expect the two sigma accuracy of the energies to be about 1.5 to 2.0 kcal/mol. It is harder to know what kind of accuracy to expect in the partition function evaluations. I would guess that the uncertainties for that are somewhere between a factor of two and ten – at least for the MC-TST case.

RESPONSE

We agree with the reviewer and have expanded the discussion of the T_1 diagnostic and possible multireference effects, supported by previous benchmark studies (Vereecken et al., 2015; Smith and Karton, 2020; Li et al., 2023; Du and Zhang, 2020). These studies provide context for the expected uncertainties of approximately 1–2 kcal mol^{-1} in calculated energies and activation barriers, depending on the reaction pathway. We have also acknowledged that possible diradical pathways in POZ decomposition were not explicitly investigated. To assess the influence of multiple conformers, we compared rate coefficients for 12 representative unimolecular reactions using multiconformer and

lowest-conformer partition functions (Table S9). The differences ranged from factors of 1.05 to 10.3, with the largest difference observed for a reaction involving 22 reactant conformers and 3 transition-state conformers, as discussed in detail in Section S8. While most MC-TST rate coefficients were lower than their lowest-conformer counterparts, a few were higher. For these reactions, the transition states had more conformers than the corresponding reactants, increasing the transition-state-to-reactant partition-function ratio ($Q_{\mathrm{TS}}/Q_{\mathrm{reactant}}$). Although the absolute rate coefficients changed, the relative ordering of competing pathways remained unchanged. Thus, the conformational treatment did not qualitatively alter the kinetic preferences or mechanistic conclusions for the pathways examined.

CHANGES TO MANUSCRIPT

Methods section, lines 166–182: "To characterize the electronic structure of the species involved in the rate coefficient calculations, coupled-cluster T_1 diagnostic values were evaluated for the key intermediates and transition states. While the POZ dissociation transition states remained within the conventional single-reference regime ($T_1 \leq 0.02$), O_3 exhibited a T_1 value of 0.0247, and the Criegee intermediates, O_5–O_9 oxygenated intermediates, and their associated transition structures exhibited T_1 values between 0.02 and 0.03 (coupled-cluster output files deposited in the Zenodo repository). These values suggest possible multireference effects and associated uncertainties in single-reference energetics, consistent with previous studies of O_3 and Criegee intermediates (Vereecken et al., 2015). Benchmark studies on Criegee chemistry have shown that certain CCSD(T)-based approaches can reproduce higher-level CCSDT(Q)/CBS reaction energies and activation barriers with sub-kcal mol^{-1} deviations for the reactions examined (Smith and Karton, 2020). Nevertheless, the accuracy of single-reference calculations depends on the electronic structure and reaction pathway, particularly for species exhibiting multireference character. For related RO_2 H-shift reactions, Li et al. (2023) reported deviations of 0.46–1.72 kcal mol^{-1} between CCSD(T)-F12 and CASPT2/CBS calculations. These literature comparisons provide an indication of the possible magnitude of uncertainties in the calculated relative energies and activation barriers of the present study, although these uncertainties may vary among reaction pathways. In addition, uncertainties associated with conformational contributions to the molecular partition functions were assessed for 12 representative unimolecular reactions, revealing variations in the calculated rate coefficients by factors of 1.05–10.3 without altering the relative ordering of the competing pathways examined (Table S9). While acknowledging these uncertainties and limitations, we find that the calculated reaction pathways and kinetic trends are consistent with the available experimental observations."

CHANGES TO SUPPLEMENT

Table S9. Comparison of unimolecular rate coefficients calculated using partition functions (Q values) that include contributions from multiple conformers and those calculated using only the lowest-energy conformers of the reactants and transition states for 12 representative reactions along the VHP-A, VHP-B, and VHP-C pathways. Rate coefficients are reported in s^{-1}.

Reaction / transition state	k (multiconformer) (s^{-1})	k (lowest conformer) (s^{-1})
VHP-A | VHP_O5_mol		
rg_7_ts	3.87×10^{-4}	1.25×10^{-3}
rg_6_ts	3.04×10^{-2}	1.25×10^{-1}
17_hsft_ts	1.63×10^{-3}	8.30×10^{-3}
VHP-B | VHP_B_mol		
14_ts	5.21×10^{-1}	5.47×10^{-1}
VHP-B | VHP_B_O5_mol		
14_ts	9.33×10^{-2}	9.85×10^{-2}
VHP-B | VHP_B_O7_mol		
rg_ts	4.47×10^{-2}	2.87×10^{-2}
VHP-C pathway to O_7 | O5-c-V		
O5_16_ts	1.01×10^{3}	6.05×10^{2}
VHP-C pathway to O_7 | O7-c-V		
O7_16_ts	4.76×10^{-4}	1.28×10^{-3}
O7_hscrambling_ts	2.10×10^{-1}	5.66×10^{-1}
VHP-C pathway to O_9 | O5-c-VI		
O5_14_TS	5.79×10^{-2}	5.94×10^{-1}
VHP-C pathway to O_9 | O7-c-VI		
rg_5_TS	1.72×10^{1}	3.89×10^{1}
rg_6_TS	1.89×10^{-2}	7.14×10^{-2}

Transition-state labels are shown as rg_7_ts, rg_6_ts, rg_ts, rg_5_TS, and rg_6_TS, which designate ring-closure pathways; 14_ts, 17_hsft_ts, O5_16_ts, O7_16_ts, and O5_14_TS, which designate the indicated hydrogen-shift pathways; and O7_hscrambling_ts, which denotes hydrogen scrambling. Identical short labels in different group rows refer to different reactions.

REVIEWER COMMENT R1.4

Meanwhile, the master equation treatment of the pressure dependence likely introduces an additional factor of two to three uncertainty, at least when the pressures of interest are far from the high-pressure limit.

RESPONSE

We thank the reviewer. To assess the sensitivity of the predicted Criegee intermediate (CI) branching fractions, we performed additional calculations by varying the pressure from 0.1 to 10 atm at 298 K

and the average downward energy transfer parameter ($\langle \Delta E \rangle_{\mathrm{down}}$) from 150 to 300 $\mathrm{cm^{-1}}$ at 1 atm, while keeping the remaining parameters unchanged. These ranges were selected to examine the sensitivity over a broad pressure interval around the reference condition of 1 atm and to variations in the energy-transfer parameter around the reference value of 225 $\mathrm{cm^{-1}}$. Varying the pressure from 0.1 to 10 atm resulted in relatively small changes in the overall branching distribution. The branching fraction of Syn-CI-1 remained around 0.7 %, while that of Syn-CI-2 increased slightly from 7.0 % to 7.1 %. Similarly, the branching fraction of Anti-CI-1 decreased from 2.9 % to 2.1 %, whereas that of Anti-CI-2 increased from 89.4 % to 90.3 %. Varying $\langle \Delta E \rangle_{\mathrm{down}}$ from 150 to 300 $\mathrm{cm^{-1}}$ at 1 atm produced even smaller changes. The branching fractions of Syn-CI-1 and Syn-CI-2 remained around 0.7 % and 7.0 %, respectively, while those of Anti-CI-1 and Anti-CI-2 remained around 2.8 % and 89.5 %, respectively. The results are summarized in Table S10. These sensitivity calculations indicate that the predicted overall branching distribution is relatively insensitive to the pressure and energy-transfer parameter variations examined. In particular, Anti-CI-2 remains the dominant product channel, accounting for approximately 89–90 % of the total CI population. Nevertheless, we acknowledge that uncertainties in the master-equation treatment may affect the absolute rate coefficients, particularly under conditions far from the high-pressure limit. We have clarified this point in the revised manuscript, and the corresponding MESMER XML file has been deposited in the Zenodo repository (https://doi.org/10.5281/zenodo.24019854).

CHANGES TO MANUSCRIPT

Methods section, lines 192–198: "To assess the sensitivity of the predicted CI branching ratios to the master-equation parameters, additional calculations were performed by varying the pressure from 0.1 to 10 atm at 298 K and the average downward energy transfer parameter ($\langle \Delta E \rangle_{\mathrm{down}}$) from 150 to 300 $\mathrm{cm^{-1}}$ at 1 atm, while keeping the remaining parameters unchanged. These ranges were selected to examine the sensitivity of the predictions over a broad pressure interval around the reference condition of 1 atm and to variations in the energy-transfer parameter around the reference value of 225 $\mathrm{cm^{-1}}$. As summarized in Table S10, the predicted branching ratios showed relatively small variations across the conditions investigated, with Anti-CI-2 remaining the dominant product channel."

CHANGES TO SUPPLEMENT

Table S10. Sensitivity of predicted Criegee intermediate branching fractions to pressure and average downward energy transfer.

Sensitivity test	Syn-CI-1 (%)	Syn-CI-2 (%)	Anti-CI-1 (%)	Anti-CI-2 (%)
Pressure variation (298 K)				
0.1 atm	0.69	7.00	2.89	89.42
1 atm	0.69	7.00	2.83	89.48
10 atm	0.63	7.05	2.06	90.25
$\langle \Delta E \rangle_{\mathrm{down}}$ **variation (1 atm, 298 K)**				
150 $\mathrm{cm^{-1}}$	0.69	7.00	2.86	89.45
225 $\mathrm{cm^{-1}}$	0.69	7.00	2.83	89.48
300 $\mathrm{cm^{-1}}$	0.68	7.00	2.79	89.53

Branching fractions are reported as percentages. Pressure sensitivity was evaluated at 298 K over the range 0.1–10 atm. Sensitivity to the average downward collisional energy-transfer parameter, $\langle \Delta E \rangle_{\mathrm{down}}$, was evaluated at 1 atm and 298 K using values of 150, 225, and 300 cm^{-1}. All branching fractions are reported to two decimal places.

REVIEWER COMMENT R1.5

It would also be useful to suggest an expected uncertainty for the M06-2X calculations used for the SI data. If this is 5 kcal/mol can all the SI pathways still be ruled out? What if it is 10 kcal/mol? In principle, you have an indication of the accuracy of the M06-2X energies for the fairly large set of stationary points where you also calculated the CCSD(T) energies.

RESPONSE

We agree with the reviewer that uncertainties associated with the M06-2X calculations should be considered when evaluating the additional pathways presented in the Supporting Information. To assess the accuracy of the calculated energies, we compared activation barriers obtained at the M06-2X and CCSD(T)-F12a levels of theory for 30 representative transition states, finding a mean absolute difference of approximately 1.1 kcal mol^{-1} and a maximum difference of 3.31 kcal mol^{-1} (Table S7). Following the reviewer's suggestion, we performed a sensitivity analysis using conventional transition-state theory at 298.15 K to estimate unimolecular rate coefficients using the original M06-2X activation Gibbs free-energy barriers and a hypothetical reduction of 4 kcal mol^{-1}. This reduction was selected based on the maximum difference observed in our comparison of the two theoretical approaches. The rate coefficients were estimated using the Eyring equation $k(T) = (k_B T/h)\exp(-\Delta G^{\ddagger}/RT)$, where k_B is the Boltzmann constant, h is Planck's constant, T is the temperature, R is the gas constant, and $\Delta G^{\ddagger}$ is the activation Gibbs free energy. Representative results for Fig. S7 are summarized in Table S8. The results indicate that, even with a 4 kcal mol^{-1} reduction in the activation barriers, the additional pathways generally retain relatively low estimated rate coefficients, with the highest value reaching approximately 8.00×10^{-2} s^{-1}. However, their possible contributions cannot be entirely excluded without considering competition with other reaction channels. We have revised the Supporting Information to acknowledge these uncertainties and removed the categorical description of all additional pathways as kinetically uncompetitive. The main manuscript focuses on the kinetically favored pathways leading to highly oxygenated organic molecule (HOM) formation, while Figs. S7–S12 present other possible pathways that may also contribute depending on their activation barriers and competing reactions.

CHANGES TO MANUSCRIPT

Results section, lines 414–419: "Among the pathways investigated following the formation of VHP-A and VHP-B, the reaction sequences considered in the present study were identified as the kinetically most favorable based on their calculated activation barriers. In comparison, the alternative reaction channels examined in Section S7 (Figs. S7a and S7b; Tables S7 and S8) generally exhibited higher activation barriers (>25 kcal mol^{-1}), suggesting that they are less likely to compete under the investigated conditions. However, their possible contributions cannot be entirely excluded, considering the uncertainties associated with the calculated activation barriers."

CHANGES TO SUPPLEMENT

Table S7. Comparison of calculated activation Gibbs free-energy barriers ($\Delta G^{\ddagger}$, kcal mol^{-1}) obtained using M06-2X/6-31G(d,p) and RHF-RCCSD(T)-F12a/VDZ-F12//M06-2X/aug-cc-pVTZ for 30 transition states.

Reactant / Intermediate	**Reaction / Transition State**	**M06-2X** $\Delta G^{\ddagger}$	**CCSD(T)-F12a** $\Delta G^{\ddagger}$	**Difference** $\Delta\Delta G^{\ddagger}$
	POZ formation			
2,5-DMF + O_3	POZ-IN formation (poz_ts_in)	8.96	10.66	+1.70
2,5-DMF + O_3	POZ-OUT formation (poz_ts_out)	11.00	12.61	+1.61
	POZ-IN decomposition			
poz_in_mol	Anti-CI-1 formation (Anti_ci_1_ts)	30.47	30.11	-0.37
poz_in_mol	Anti-CI-2 formation (Anti_ci_2_ts)	24.47	24.32	-0.15
	POZ-OUT decomposition			
poz_out_mol	Syn-CI-1 formation (syn_ci_1_ts)	26.74	26.46	-0.28
poz_out_mol	Syn-CI-2 formation (syn_ci_2_ts)	22.03	21.91	-0.12
	Syn-CI-1			
syn_ci_1_mol	di_ox_ts	12.05	11.93	-0.12
syn_ci_1_mol	1,4-H shift (14_ts)	17.95	15.25	-2.70
	Syn-CI-2			
syn_ci_2_mol	di_ox_ts	18.65	18.03	-0.62
	Anti-CI-1			
Anti_ci_1_mol	1,6-H shift (16_ts)	23.90	20.61	-3.30
Anti_ci_1_mol	soz_ts	8.25	8.47	+0.23
	Anti-CI-2			
Anti_ci_2_mol	1,4-H shift (14_ts)	21.13	19.27	-1.87
	VHP-A			
VHP_O5_mol	Ring closure (rg_7_ts)	21.27	21.00	-0.27
VHP_O5_mol	Ring closure (rg_6_ts)	18.14	18.34	+0.20
VHP_O5_mol	1,7-H shift (17_hsft_ts)	25.60	22.82	-2.78

Table S7. Continued.

Reactant / Intermediate	**Reaction / Transition State**	**M06-2X** $\Delta G^{\ddagger}$	**CCSD(T)-F12a** $\Delta G^{\ddagger}$	**Difference** $\Delta\Delta G^{\ddagger}$
	VHP-B			
VHP_B_O5_mol(6)	1,4-H shift (14_ts)	23.92	22.83	-1.09
VHP_B_O7_mol(21)	Ring closure (rg_ts)	22.95	19.64	**-3.31**
	VHP-C O5-V pathway			
VHP_C_VO5_mol(4)	1,6-H shift (16_ts)	18.02	16.36	-1.66
VHP_C_VO7_mol(10)	1,6-H shift (16_ts)	25.91	24.61	-1.30
VHP_C_VO7_mol(10)	1,8-H scrambling (18_hscram_ts)	19.47	22.52	+3.05
	VHP-C O5-VI pathway			
VHP_C_VIO5_mol(1)	1,4-H shift (14_ts)	24.71	21.85	-2.86
VHP_C_VIO7_mol(2)	Five-membered ring closure (rg_5_ts)	15.74	15.56	-0.18
VHP_C_VIO7_mol(2)	Six-membered ring closure (rg_6_ts)	19.13	19.24	+0.10
	2,5-DMF + OH			
2,5-DMF + OH	1,4-H abstraction (25_dmf_1_4_h_abs_ts)	7.61	7.19	-0.42
2,5-DMF + OH	2,5-OH addition (25_dmf_2_5_oh_ad_ts)	3.06	3.60	+0.53
2,5-DMF + OH	3,4-OH addition (25_dmf_3_4_oh_ad_ts)	6.08	6.33	+0.25
	OH addition: Same-side O_2 addition			
25_DMF_3OH_OO_rad	RF_5_TS	15.96	15.91	-0.05
25_DMF_3OH_OO_rad	RF_6_TS	18.26	18.00	-0.26
	OH addition: Opposite-side O_2 addition			
25_DMF_3OH_OO_rad	RF_5_TS	21.19	21.01	-0.18
25_DMF_3OH_OO_rad	RF_6_TS	22.57	22.27	-0.29

Differences are calculated as $\Delta\Delta G^{\ddagger} = \Delta G^{\ddagger}_{\mathrm{CCSD(T)-F12a}} - \Delta G^{\ddagger}_{\mathrm{M06-2X}}$; negative values indicate lower activation barriers at the CCSD(T)-F12a level, whereas positive values indicate higher barriers. All values are in kcal mol^{-1}.

Table S8. Sensitivity analysis of the calculated unimolecular rate coefficients for selected additional reaction pathways shown in Fig. S7. Rate coefficients were estimated at 298.15 K using the original activation Gibbs free-energy barriers calculated at the M06-2X/6-31G(d,p) level of theory and after a hypothetical reduction of 4 kcal mol^{-1} in these barriers.

Initial structure	Reaction	$\Delta G^{\ddagger}$ (kcal mol^{-1})	k_{original} (s^{-1})	k_{-4} (s^{-1})
Figure S7a: VHP-A-derived pathways				
$C_6H_7O_7$-IIa	1,4-H shift	25.18	2.17×10^{-6}	1.86×10^{-3}
$C_6H_7O_7$-IIb	1,3-H shift	46.73	3.47×10^{-22}	2.97×10^{-19}
$C_6H_7O_7$-IIb	1,5-H shift	35.26	8.86×10^{-14}	7.58×10^{-11}
$C_6H_7O_7$-IIIa	1,6-H shift	51.07	2.28×10^{-25}	1.95×10^{-22}
$C_6H_7O_7$-IIIa	Ring formation	35.97	2.67×10^{-14}	2.28×10^{-11}
Figure S7b: VHP-B-derived pathways				
$C_6H_7O_5$-IVa	1,7-H shift	49.34	4.23×10^{-24}	3.62×10^{-21}
$C_6H_7O_5$-IVa	1,5-H shift	29.60	1.25×10^{-9}	1.07×10^{-6}
$C_6H_7O_5$-IVa	1,4-H shift	23.91	1.85×10^{-5}	1.58×10^{-2}
$C_6H_7O_7$-IVb	Ring formation	22.95	9.35×10^{-5}	8.00×10^{-2}
$C_6H_7O_7$-IVb	1,8-H shift	30.24	4.24×10^{-10}	3.63×10^{-7}

Rate coefficients were calculated at 298.15 K using conventional transition-state theory with the original M06-2X/6-31G(d,p) activation Gibbs free-energy barriers and a hypothetical reduction of 4 kcal mol^{-1}. The column k_{original} represents the rate coefficients obtained using the original barriers, whereas k_{-4} represents those obtained after reducing the barriers by 4 kcal mol^{-1}. The rate estimates do not include explicit tunneling corrections or multiconformer contributions.

REVIEWER COMMENT R1.6

It appears that the authors calculate the rate constant for O_3 to add 25DMF. Those calculated rates should be compared to the literature rates. That comparison would provide some qualitative indication of the accuracy of their methods. Perhaps the calculated number is reported on line 41 of the SI, but that should be made more clear.

RESPONSE

We thank the reviewer for this suggestion. We agree that comparison of the calculated O_3+2,5-DMF rate coefficients with the available experimental measurements provides a useful assessment of the performance and limitations of the theoretical treatment. In the revised calculations, two O_3-addition pathways leading to different primary ozonide orientations (POZ-IN and POZ-OUT) were characterized. After application of the revised reaction-path symmetry factor, the calculated rate coefficients are 4.02×10^{-15} and 3.37×10^{-16} cm^3 molecule^{-1} s^{-1} for formation of POZ-IN and POZ-OUT, respectively. Experimentally, Matsumoto (2011) reported a rate coefficient of $(4.2 \pm 0.9) \times 10^{-16}$ cm^3 molecule^{-1} s^{-1} for the O_3+2,5-DMF reaction, while the more recent measurements of Illmann and Rösgen (2024) yielded $(3.3 \pm 1.0) \times 10^{-16}$ cm^3 molecule^{-1} s^{-1}. The calculated rate coefficient for the POZ-OUT pathway is therefore in close agreement with the available experimental values, whereas the calculated POZ-IN rate coefficient is found to be approximately one order of magnitude larger. The total calculated rate coefficient for O_3 + 2,5-DMF, summing both addition orientations, is $k_{\mathrm{total}} = k_{\mathrm{POZ\text{-}IN}} + k_{\mathrm{POZ\text{-}OUT}} = 4.36 \times 10^{-15}$ cm^3 molecule^{-1} s^{-1}.

CHANGES TO MANUSCRIPT

Results section, lines 361–368: "In the present study, two distinct orientations of O_3 addition to 2,5-DMF were investigated, leading to the formation of primary ozonides denoted as POZ-IN and POZ-OUT, with calculated rate coefficients of 4.02×10^{-15} and 3.37×10^{-16} cm^3 molecule^{-1} s^{-1}, respectively, summing to a total rate coefficient of 4.36×10^{-15} cm^3 molecule^{-1} s^{-1} for O_3 + 2,5-DMF, approximately one order of magnitude higher than the experimental values. The calculated rate coefficient for the POZ-OUT pathway is in close agreement with the experimental values reported by Matsumoto (2011) and Illmann and Rösgen (2024), who determined rate coefficients of $(4.2 \pm 0.9) \times 10^{-16}$ and $(3.3 \pm 1.0) \times 10^{-16}$ cm^3 molecule^{-1} s^{-1}, respectively, for the reaction of O_3 with 2,5-DMF. In contrast, the calculated rate coefficient for the POZ-IN pathway, and consequently the total rate coefficient, was found to be approximately one order of magnitude higher than the experimental values."

REVIEWER COMMENT R1.7

It is unclear to me how the green contribution in Fig. 2 b is obtained separately from the gray contribution. It would be helpful to have some specification of how that is done.

RESPONSE

We appreciate the reviewer's request for clarification. The spectra were recorded with a Thermo Orbitrap Exploris 240 mass spectrometer, whose very high mass resolving power allows peaks to be identified clearly, even when they lie only a few mDa apart. Fig. R1 shows two accretion products, $C_{10}H_{14}O_6$ and $C_{10}H_{12}O_8$: each assigned peak is cleanly separated from the nearest unassigned peak. We have also clarified this in the Fig. 2 caption.

CHANGES TO MANUSCRIPT

Fig. 2 caption: Fig. 2 caption now reads: "...O_3-derived monomers ($C_6H_7O_x$) are shown in yellow, OH-derived monomers ($C_6H_9O_x$) in blue, and accretion products in green; these are the peaks confirmed and formula-assigned during data processing. Grey peaks show unassigned signal, including unmatched product peaks and known instrument background." The in-figure legend label for the grey category was likewise changed from "Background" to "Unassigned", since the grey signal is not exclusively instrument background.

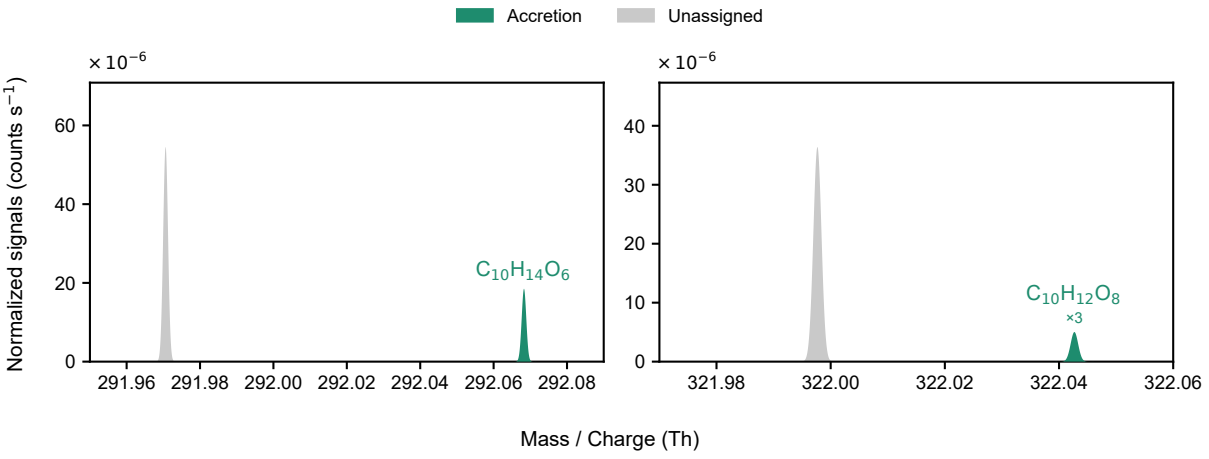


Fig. R1. High-resolution NO_3^- CIMS spectra around two accretion products, (left) $C_{10}H_{14}O_6$ and (right) $C_{10}H_{12}O_8$ (shown $\times 3$). Peak labels indicate assigned neutral molecular compositions (NO_3^- adduct excluded). The formula-assigned peaks (green) are clearly resolved from the neighbouring unassigned peaks (grey), which lie only 0.098 and 0.045 Th away, respectively.

REVIEWER COMMENT R1.8

It seems odd to me that no mention is made in lines 217 to 224 of the increased $C_6H_7O_8$ from the O_3 pathway. On line 222, the authors mention an elevated $C_5H_7O_7$ signal for the long timescale experiments. But the signals seem to be ~250 in Fig. 2a and ~200 in Fig. 2b. Thus, I am confused by that statement.

RESPONSE

We thank the reviewer for pointing this out. $C_6H_7O_8$ is indeed present at Δt = 7 s (listed in Table 2) and is in fact the most intense of the three ozonolysis-derived HOM monomers at this residence time, more intense than $C_6H_7O_7$, which was not mentioned in the previous version; we have corrected the text in the revised version to list all three monomers ($C_6H_7O_8$, $C_6H_7O_7$, $C_6H_7O_9$) in order of decreasing intensity. We have rechecked the signal intensity of $C_5H_7O_7$ (m/z 241.0075) and found that it is higher at Δt = 0.8 s (205×10^{-6}) than at Δt = 7 s (114×10^{-6}), as pointed out by the reviewer, i.e. it is not elevated at the longer residence time. We have removed this claim; most of the other signals, including $C_6H_{10}O_6$ and $C_6H_{10}O_8$, are present with higher intensity at Δt = 7 s.

CHANGES TO MANUSCRIPT

Results section, lines 240–249: Results section, Δt = 7 s paragraph: (1) now lists all three ozonolysis-derived monomers, "...the ozonolysis-derived $C_6H_7O_8$, $C_6H_7O_7$, and $C_6H_7O_9$ radicals are also present, in order of decreasing intensity." (2) the incorrect $C_5H_7O_7$ claim removed: "The prominent closed-shell products $C_6H_{10}O_6$ and $C_6H_{10}O_8$ indicate a contribution from bimolecular termination at $\Delta t = 7$ s. These formulas are consistent with RO_2 + HO_2 termination (ROOH); however, mass spectrometry alone cannot distinguish isomeric structures, and an alcohol/carbonyl pair formed via the Russell RO_2 + RO_2 self- or cross-reaction (Russell, 1957) remains an equally plausible contributor to the same nominal composition."

REVIEWER COMMENT R1.9

In Fig. 6, key intermediates are said to be highlighted in red. I am puzzled as to what makes those intermediates key? For example, the branching to VHP-A relative to the dioxirane channel next to it is less than 1%. How then is that a key channel? To make matters worse, they predict only a 5% branching to Syn-CI-1, which just adds to the confusion regarding how VHP-A can be a key intermediate.

RESPONSE

We agree with the reviewer that referring to the intermediates highlighted in red as "key intermediates" could incorrectly imply that they represent the dominant reaction channels. This was not our intention. VHP-A was highlighted because it provides a mechanistic connection between the CI-1 pathway and the subsequent radical reaction sequence leading to the experimentally observed HOMs, rather than because it represents a major branching channel. We have revised the figure and accompanying text to distinguish intermediates and pathways relevant to HOM formation from the quantitatively dominant reaction channels.

CHANGES TO MANUSCRIPT

Fig. 6 caption: New caption: "Ozonolysis of 2,5-DMF showing the formation of two primary ozonides, POZ-IN and POZ-OUT, followed by their decomposition into Anti-CI-1 and Anti-CI-2, and Syn-CI-1 and Syn-CI-2, respectively. The subsequent unimolecular reaction pathways include dioxirane formation and a 1,4-H shift for Syn-CI-1; SOZ formation and a concerted 1,6-H shift with cyclization for Anti-CI-1; dioxirane formation for Syn-CI-2; and a 1,4-H shift for Anti-CI-2. Rate coefficients (k, s^{-1} for unimolecular reactions

and cm^3 molecule^{-1} s^{-1} for bimolecular reactions) and barrier heights ($\Delta G^{\ddagger}$, kcal mol^{-1}) were calculated at the RHF-RCCSD(T)-F12a/VDZ-F12//M06-2X/aug-cc-pVTZ level of theory. Colour code: purple indicates unimolecular rate coefficients and activation barriers, while blue indicates bimolecular rate coefficients. Red highlights intermediates that undergo subsequent reaction steps leading toward HOM formation, while blue oxygen atoms indicate those originating from O_3."

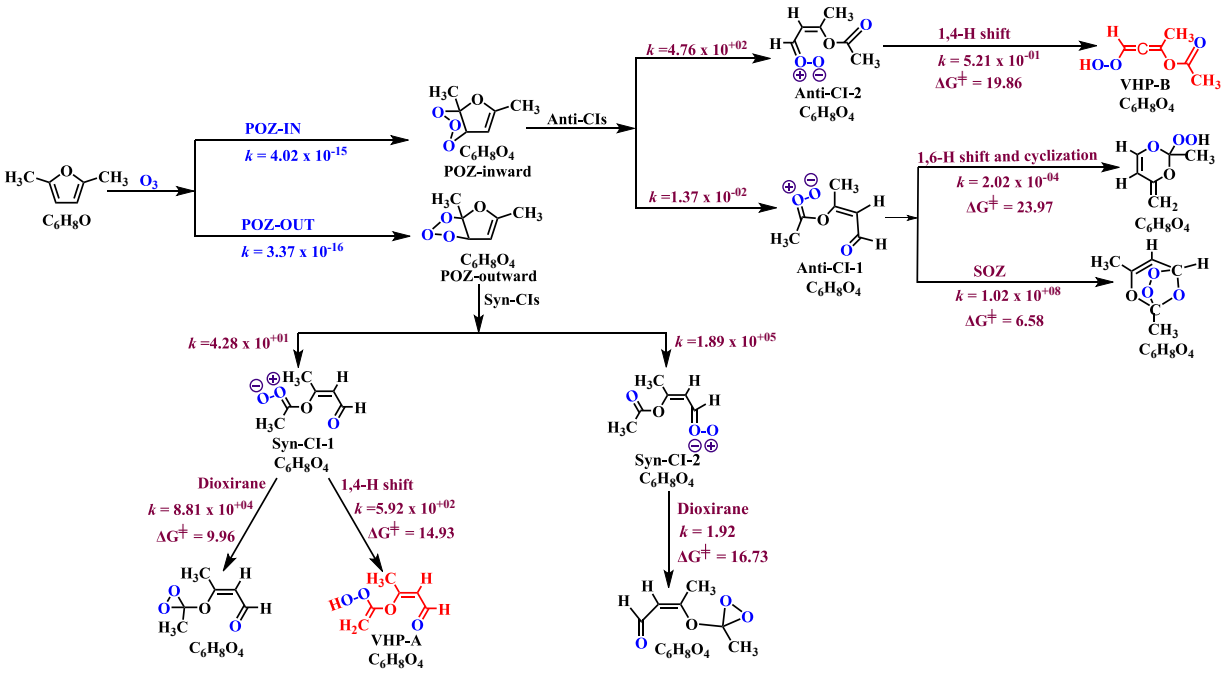


Fig. 6. Ozonolysis of 2,5-DMF showing the formation of two primary ozonides, POZ-IN and POZ-OUT, followed by their decomposition into Anti-CI-1 and Anti-CI-2, and Syn-CI-1 and Syn-CI-2, respectively. The subsequent unimolecular reaction pathways include dioxirane formation and a 1,4-H shift for Syn-CI-1; SOZ formation and a concerted 1,6-H shift with cyclization for Anti-CI-1; dioxirane formation for Syn-CI-2; and a 1,4-H shift for Anti-CI-2. Rate coefficients (k, s^{-1} for unimolecular reactions and cm^3 molecule^{-1} s^{-1} for bimolecular reactions) and barrier heights ($\Delta G^{\ddagger}$, kcal mol^{-1}) were calculated at the RHF-RCCSD(T)-F12a/VDZ-F12//M06-2X/aug-cc-pVTZ level of theory. Colour code: purple indicates unimolecular rate coefficients and activation barriers, while blue indicates bimolecular rate coefficients. Red highlights intermediates that undergo subsequent reaction steps leading toward HOM formation, while blue oxygen atoms indicate those originating from O_3.

REVIEWER COMMENT R1.10

Should there also be a diradical channel for the decomposition? Perhaps that channel might be 10% of the flux to CI-1 and CI-2. But that would still make it more than the flux to VHP-A. Are the authors aware of some data that says a diradical channel would be irrelevant for 25DMF ozonolysis?

RESPONSE

We thank the reviewer for raising this point. A biradical pathway has been proposed previously for gas-phase ozonolysis. For example, Kühne et al. (1980) discussed an O'Neal–Blumstein biradical pathway in cis-2-butene ozonolysis but also identified the Criegee-type pathway as the dominant reaction channel. In the present study, we did not explicitly investigate the biradical pathway, as our focus was on Criegee-intermediate chemistry and the subsequent reaction pathways leading to the observed highly oxygenated products. For 2,5-DMF ozonolysis, Illmann and Rösgen (2024) reported no experimental indication of products arising from the stepwise O'Neal–Blumstein POZ dissociation

mechanism. However, this observation does not exclude a contribution from such a pathway, and its branching fraction cannot be determined from the present calculations. Therefore, we cannot rule out the possibility raised by the reviewer that a biradical channel could contribute more substantially than the pathway leading to VHP-A. We have clarified this limitation in the revised manuscript. We also emphasize that VHP-A was investigated because it represents a mechanistically relevant route toward HOM formation, rather than because it constitutes a major POZ decomposition channel.

CHANGES TO MANUSCRIPT

Results section, lines 375–380: "In addition to the Criegee-intermediate-forming pathways, an alternative stepwise POZ decomposition mechanism involving biradical intermediates, known as the O'Neal–Blumstein pathway, has been discussed for cis-2-butene ozonolysis (Kühne et al., 1980). This pathway was not explicitly investigated in the present study, as the primary focus was on Criegee-intermediate chemistry and its contribution to HOM formation. Furthermore, Illmann and Rösgen (2024) reported no experimental evidence for products arising from this alternative pathway during 2,5-DMF ozonolysis. Therefore, its potential contribution to POZ decomposition remains unquantified in the present study."

REVIEWER COMMENT R1.11

The IRC calculations connect to the syn CI-1 and CI-2 conformers. It would be helpful for the authors to say what they take this to mean for the formation of the anti CI-1 and anti CI-2 conformers? They show the product of Anti-CI-2 as being a key intermediate in Fig. 6. So apparently they believe that there is still some possibility for forming Anti-CI-2. Some statement should be made as to how the anti-conformers might be formed. Presumably some inspection of the TSs for forming the CIs would indicate that the torsional partition function likely contains some probability of being in a torsional state that would correlate with the Anti-CIs.

RESPONSE

We thank the reviewer for raising this point. In the original calculations, POZ decomposition was characterized from the outward-oriented POZ conformer, for which the IRC calculations led to the Syn-CI conformers, while the possible formation of the corresponding Anti-CI conformers was considered based on previous understanding of CI formation during ozonolysis. Prompted by the reviewer's comment, we examined the conformational dependence of POZ decomposition in greater detail. The additional IRC calculations indicate that decomposition from the inward-oriented, global-minimum POZ conformer leads to the Anti-CI conformers, whereas decomposition from the outward-oriented POZ conformer leads to the Syn-CI conformers. Similar conformer-dependent Syn/Anti CI formation has been discussed in previous studies of ozonolysis (Wang and Wang, 2017).
We have therefore included these additional pathways and their corresponding rate coefficients in the revised manuscript. This analysis provides a possible mechanistic explanation for the formation of Anti-CI-1 and Anti-CI-2 during POZ decomposition and improves the interpretation of subsequent CI chemistry.

CHANGES TO MANUSCRIPT

Results section, lines 361–371: "In the present study, two distinct orientations of O_3 addition to 2,5-DMF were investigated, leading to the formation of primary ozonides denoted as POZ-IN and POZ-OUT, with calculated rate coefficients of 4.02×10^{-15} and 3.37×10^{-16} cm^3 $molecule^{-1}$ s^{-1}, respectively, summing to a total rate coefficient of 4.36×10^{-15} cm^3 $molecule^{-1}$ s^{-1} for O_3 + 2,5-DMF, approximately one order of magnitude higher than the experimental values. The calculated rate coefficient for the POZ-OUT pathway is in close agreement with the experimental values reported by Matsumoto (2011) and Illmann and Rösgen (2024), who determined

rate coefficients of $(4.2 \pm 0.9) \times 10^{-16}$ and $(3.3 \pm 1.0) \times 10^{-16}$ cm^3 molecule^{-1} s^{-1}, respectively, for the reaction of O_3 with 2,5-DMF. In contrast, the calculated rate coefficient for the POZ-IN pathway, and consequently the total rate coefficient, was found to be approximately one order of magnitude higher than the experimental values. Subsequent POZ decomposition leads to the formation of the Criegee intermediates CI-1 and CI-2, where the POZ-IN yields the Anti-CI conformers, whereas the POZ-OUT yields the Syn-CI conformers. Similar conformer-dependent CI formation has been discussed for sabinene ozonolysis (Wang and Wang, 2017)."

REVIEWER COMMENT R1.12

Some comment should be made as to whether or not the rates in Fig. 8 are fast enough to allow much production of the HOMs on the 0.8 s timescale or even on the 7 s timescale. I think the answer to that question depends to some extent on what the uncertainty in the rate predictions is. Do the simulations indicate that Anti-CI-2A is required in order to form any HOMs on the experimental timescales?

RESPONSE

We thank the reviewer for this comment. In response, we have expanded the kinetic analysis and clarified the discussion of HOM formation within the experimental residence times. In the previously submitted manuscript, the kinetic treatment was limited because the formation pathways and corresponding rate coefficients for all relevant Criegee intermediates were not available. In the revised study, we have connected the calculated reaction pathways from POZ decomposition through Syn-CI-1, Syn-CI-2, Anti-CI-1, and Anti-CI-2 to the subsequent formation of O_7 species and performed kinetic simulations at the experimental residence times of 0.8 and 7 s. The simulations indicate that O_7 RO_2 can form within 0.8 s through these conventional CI pathways, with a time-averaged VHP-B-O_7 concentration of 2.13×10^7 molecules cm^{-3} at 0.8 s. Additional simulations using different random seeds (11752, 26138, 11284, and 21542) yielded concentrations of the same order of magnitude, approximately 10^7 molecules cm^{-3} at 0.8 s and 10^9 molecules cm^{-3} at 7 s. These results indicate that Anti-CI-2A is not required to explain O_7 formation within the investigated experimental timescales. However, the investigated pathways beyond O_7 involve relatively high calculated activation barriers and are unlikely to contribute substantially to O_9 formation within the 0.8 s experimental residence time. This motivated us to investigate Anti-CI-2A as a possible alternative route toward the experimentally observed O_9 species. The present simulations therefore support O_7 formation through the conventional CI pathways, while the contribution of Anti-CI-2A to O_9 formation remains to be established. The corresponding kinetic reaction steps have been added to Section S6.3 of the Supporting Information (Reaction Scheme 4), and the simulated O_7 concentrations at the experimental residence times are summarized in Table S4.

CHANGES TO MANUSCRIPT

Results section, lines 419–426: "To further assess the feasibility of O_7 RO_2 formation within the experimental residence times, kinetic simulations were performed using the reaction sequences presented in Figs. 6 and 8a–b, with initial precursor concentrations corresponding to the 0.8 and 7 s experimental conditions. The simulations showed that VHP-B_O_7 ($C_6H_7O_7$-b-IV) could form within the experimental residence time of 0.8 s, with time-averaged concentrations of approximately 10^7 molecules cm^{-3} at 0.8 s and 10^9 molecules cm^{-3} at 7 s (Section S6.3, Reaction Scheme 4 and Table S4). However, the investigated pathways beyond O_7 involve relatively high calculated activation barriers, suggesting that they are unlikely to contribute substantially to the observed O_9 formation within 0.8 s. This motivated us to investigate other possible pathways that could account for the observed O_9 formation within the experimental residence time of 0.8 s."

REVIEWER COMMENT R1.13

On p. 21, the contrast in lowest conformer rates and IRC connected rates suggests a possible issue. What if the lowest energy reactant conformer is connected to a much higher barrier conformer and the conformational dynamics is very slow. Then, if all the population is in the low enough reactant conformer, the rate could be much slower. This sort of issue could readily be resolved by simply determining the barriers and rates for the conformational dynamics in the reactant, which are probably rapid enough to remove any of these ambiguities. The contrast they present really does not resolve the issue.

RESPONSE

We agree with the reviewer that the comparison between the lowest-energy reactant conformer and the IRC-connected conformer does not establish rapid conformational equilibration. Following the reviewer's suggestion, we performed additional calculations to investigate the rotational transition state connecting these conformers. The estimated Gibbs free-energy barrier for conformational interconversion was approximately 10.09 kcal mol^{-1}. Using the Eyring equation at 298.15 K, the corresponding rate coefficient was estimated to be 2.49×10^5 s^{-1}, suggesting that the conformational interconversion could occur relatively rapidly and facilitate access to the reactive IRC-connected geometry. We have revised the manuscript accordingly, and the corresponding calculation files have been deposited in the Zenodo repository (https://doi.org/10.5281/zenodo.24019854).

CHANGES TO MANUSCRIPT

Results section, lines 438–446: "Both sets of calculated rate coefficients indicate that the 1,6-hydrogen shift is intrinsically fast and is favored over the competing five-membered ring closure. The effective rate of VHP-C formation also depends on the interconversion between the lowest-energy and IRC-connected Anti-CI-2A conformers. To investigate this interconversion, additional calculations were performed to explore the rotational transition state, yielding an approximate Gibbs free-energy barrier of 10.09 kcal mol^{-1}. Using the Eyring equation at 298.15 K, the corresponding rate coefficient was estimated to be 2.49×10^5 s^{-1}, suggesting that conformational interconversion could occur relatively rapidly and facilitate access to the reactive IRC-connected geometry. Although the exact quantitative rate can vary with the computational method, this estimate supports the possibility of rapid conformational interconversion."

REVIEWER COMMENT R1.14

Are $C_6H_7O_3$-V and $C_6H_7O_3$-VI different structures, or just different depictions of the same structure? If the latter, it would be better to just indicate the resonance with a standard curved resonance bond across the two bonds (i.e., just like in their depiction of VHP-C) and then connect the subsequent V and VI species to that one resonance structure. To me, giving the same species two different labels is confusing. Furthermore, the terminal O is another part of that resonance and the resonance bond should extend to it. Similar comments could be made about a variety of other structures in their schematics. E.g., the $C_6H_7O_3$ structures in Figs. 8a and 8b should include a resonance with the neighboring C=O.

RESPONSE

We thank the reviewer for this helpful suggestion. We agree that $C_6H_7O_3$-V and $C_6H_7O_3$-VI represent different resonance structures of the same intermediate rather than distinct chemical species, and that assigning separate labels could lead to confusion. Accordingly, we have revised the reaction schemes by representing these structures as a single intermediate, $C_6H_7O_3$-a, and connecting the subsequent reaction pathways to this common structure. We have also corrected the resonance representations,

including the delocalization involving the terminal oxygen atom, and revised the corresponding structures in Figs. 8a and 8b to indicate resonance with the neighboring carbonyl group. Similar corrections have been made to the other relevant structures throughout the reaction schemes to ensure consistency and clarity.

CHANGES TO MANUSCRIPT

Reaction schemes revised: $C_6H_7O_3$-V and $C_6H_7O_3$-VI are different resonating structures of a single intermediate, $C_6H_7O_3$-a, depicted with a standard curved resonance bond extended to the terminal O; Figs. 8a, 8b and 9, and the equivalent structures elsewhere in the reaction schemes, revised to show resonance with the neighboring carbonyl group.

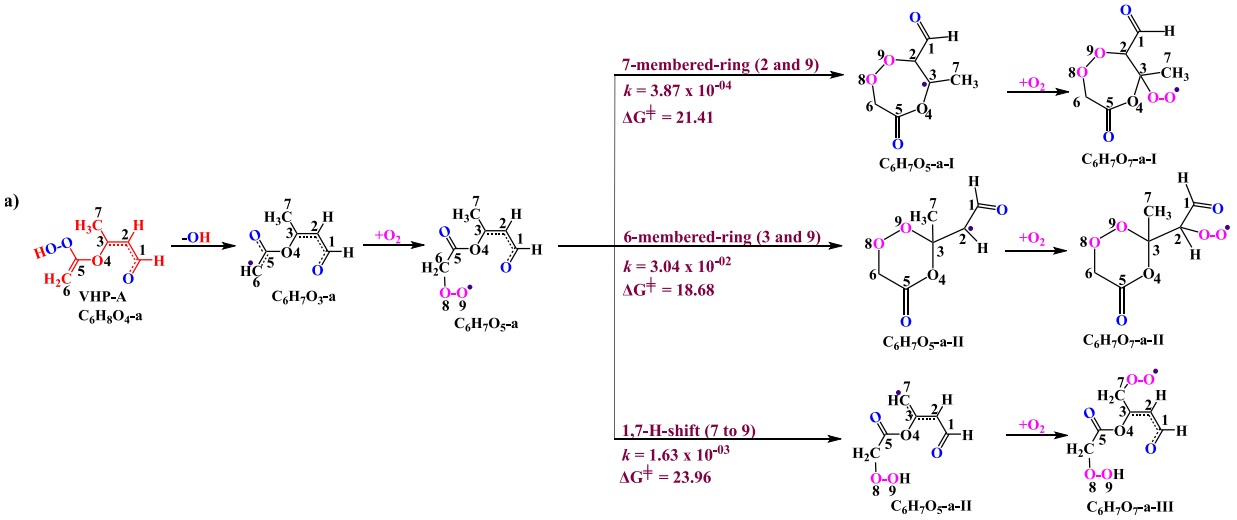


Fig. 8a. Reaction pathways for the formation of HOMs up to O_7 species initiated by (a) VHP-A produced from Syn-CI-1 and (b) VHP-B produced from Anti-CI-2, showing the key intermediates and product-forming steps. Rate coefficients (k, s^{-1}) and barrier heights ($\Delta G^{\ddagger}$, kcal mol^{-1}) were calculated at the ROHF-RCCSD(T)-F12a/VDZ-F12//M06-2X/aug-cc-pVTZ level of theory. Colour code: The red structure denotes the starting intermediate from which all pathways originate. Blue oxygen atoms indicate those originating from O_3, while pink oxygen atoms represent O_2 addition.

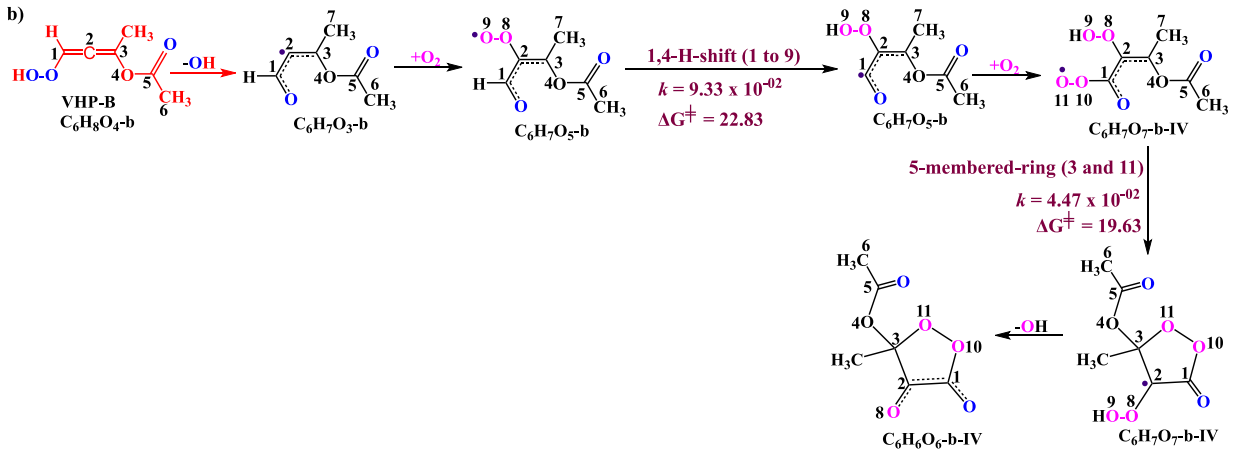


Fig. 8b. Reaction pathways for the formation of HOMs up to O_7 species initiated by (a) VHP-A produced from Syn-CI-1 and (b) VHP-B produced from Anti-CI-2, showing the key intermediates and product-forming steps. Rate coefficients (k, s^{-1}) and barrier heights ($\Delta G^{\ddagger}$, kcal mol^{-1}) were calculated at the ROHF-RCCSD(T)-F12a/VDZ-F12//M06-2X/aug-cc-pVTZ level of theory. Colour code: The red structure denotes the starting intermediate from which all pathways originate. Blue oxygen atoms indicate those originating from O_3, while pink oxygen atoms represent O_2 addition.

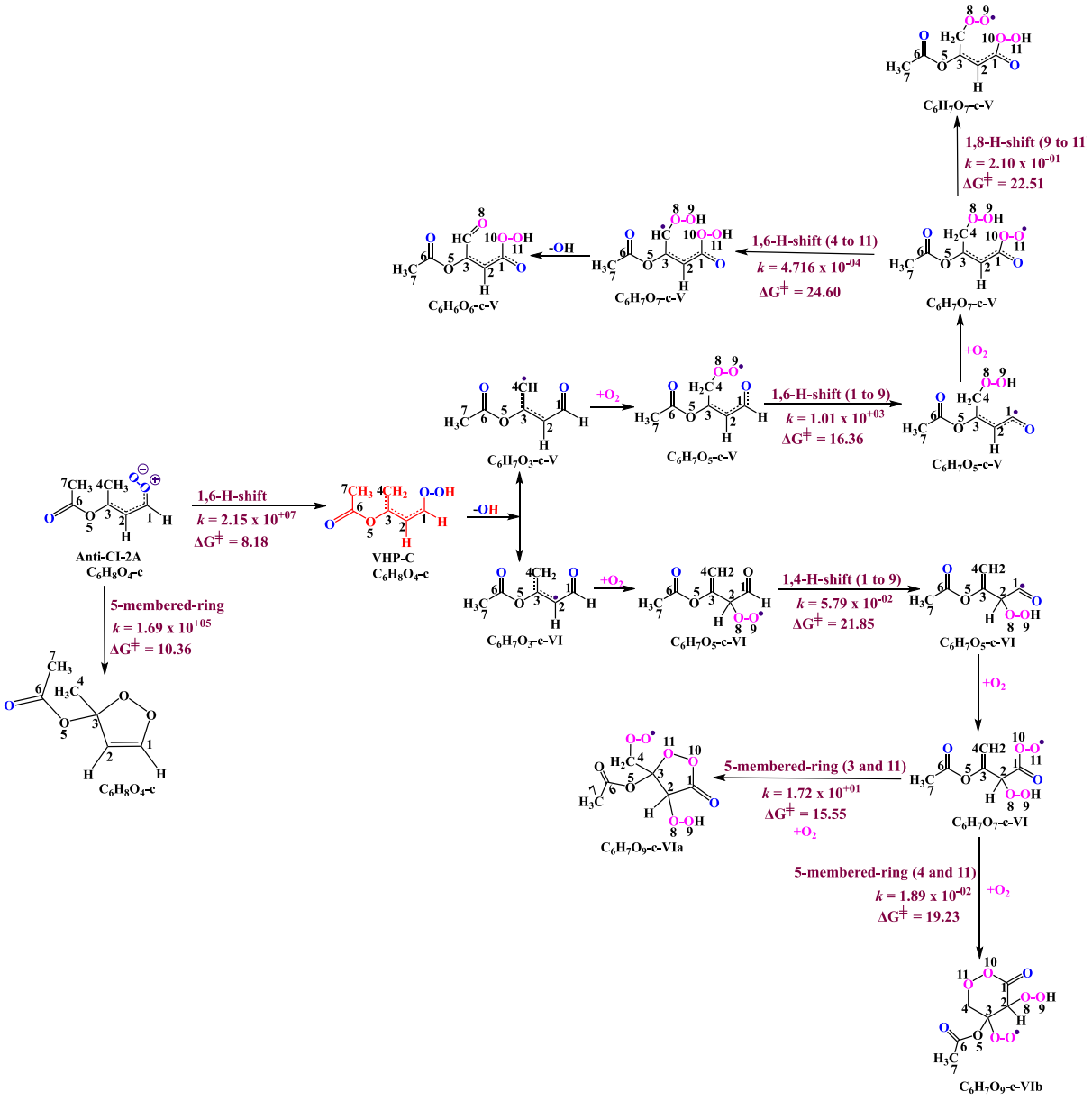


Fig. 9. Reaction pathway for the formation of HOMs up to O_9 species initiated by the Anti-CI-2A geometry, showing the key intermediates and product-forming steps. Rate coefficients (k, s^{-1}) and barrier heights ($\Delta G^{\ddagger}$, kcal mol^{-1}) were calculated at the ROHF-RCCSD(T)-F12a/VDZ-F12//M06-2X/aug-cc-pVTZ level of theory. Colour code: The red structure denotes the intermediate VHP-C from which all pathways originate. Blue oxygen atoms indicate those originating from O_3, while pink oxygen atoms represent O_2 addition.

REVIEWER COMMENT R1.15

In each of the VHP dissociations, the OH fragment arising from the OO fission could have reattached to the new C radical site (in one resonance form) in a roaming process to form hydroxyketones. This process was seen to be important in calculations for ozonolysis of alpha-pinene (J. Phys. Chem. A,

127, 10657, 2023) and directly observed in methyl ethyl CI (J. Am. Chem. Soc. 145, 19405, 2023). Some comments on the expected relevance of such roaming processes to the HOM formations would be helpful.

RESPONSE

We thank the reviewer for pointing out this possibility. We agree that following VHP O–O bond cleavage, the departing OH fragment may undergo roaming and reattach to a carbon-centered radical site, providing a competing route to hydroxyketone formation (Klippenstein and Elliott, 2023; Liu et al., 2023). If operative in the present system, such a pathway could reduce the fraction of VHP-derived radicals available for O_2 addition and subsequent autoxidation toward HOM formation. However, OH roaming was not explicitly investigated in the present calculations, and its quantitative contribution relative to the conventional OH-elimination pathways cannot be determined. We have therefore added a discussion acknowledging this possible competing mechanism and its potential influence on HOM formation.

CHANGES TO MANUSCRIPT

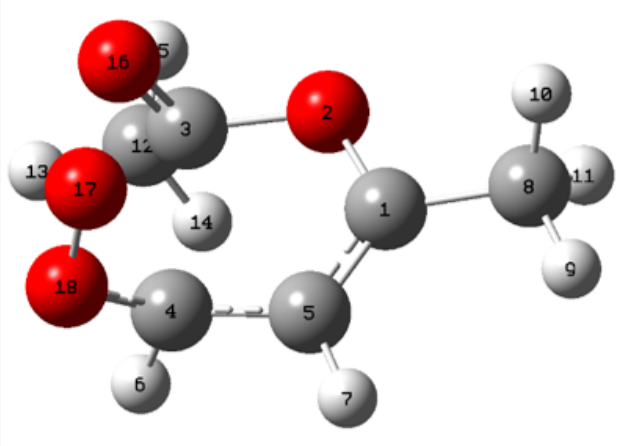
Results section, lines 393–397: "Previous studies have also reported OH roaming during vinyl hydroperoxide (VHP) decomposition, in which the departing OH fragment can reattach to the molecular framework, leading to closed-shell products, such as hydroxyketones (Klippenstein and Elliott, 2023; Liu et al., 2023). In the present study, we focused on the mechanistic analysis of conventional OH-elimination pathways and the subsequent reactions of the resulting radicals without explicitly accounting for possible OH roaming contributions."

REVIEWER COMMENT R1.16

The discussion on the bottom of p. 21, presumes strong reliance on the appropriateness of IRC calculations in identifying final products. Transition state theory does not say that IRCs are followed out to products. The passage through the TS's will occur over a distribution of torsional states. There are then two key questions. (i) Do different torsional values at the TS correlate with different conformers of the CIs (e.g., Syn-CI-2 vs. Anti-CI-2 vs. Anti-CI-2A)? (ii) If there are torsional values that correlate with Anti-CI-2A, does one expect a reasonable population of those torsional values? The first question could be reasonably addressed with simple optimizations that start from a specific torsional value and a slight kick in the direction of the products. Do you see different product CI conformers when you do that?

RESPONSE

We thank the reviewer for suggesting this additional test to better understand the possible formation of different CI conformers. In the revised calculations, we were able to locate transition states leading directly to Anti-CI-1 and Anti-CI-2, which had not been identified in the original manuscript.
Following the reviewer's suggestion, we further examined the possible formation of Anti-CI-2A by systematically varying the torsional angle of the newly identified Anti-CI-2-forming transition-state structure. The original dihedral angle between atom number 8, 1, 5 and 7 was $-2.35°$, shown in figure below.



Then, most of the modified structures relaxed to different closed-shell products following product-side displacement and subsequent unconstrained geometry optimization. However, at dihedral angles of $-149.98°$ and $-142.35°$, the optimizations resulted in the Anti-CI-2A conformer. These observations suggest that Anti-CI-2A may be accessible from certain torsional configurations. However, we acknowledge that the present calculations do not establish the exact mechanism or relative contribution of Anti-CI-2A formation. Since this conformer provides a plausible pathway toward the formation of O_9 products, we have discussed its subsequent reaction chemistry in our mechanistic investigation while acknowledging that its precise formation pathway remains uncertain and cannot be fully resolved within the scope of the present study.

CHANGES TO MANUSCRIPT

Results section, lines 361–371: "In the present study, two distinct orientations of O_3 addition to 2,5-DMF were investigated, leading to the formation of primary ozonides denoted as POZ-IN and POZ-OUT, with calculated rate coefficients of 4.02×10^{-15} and 3.37×10^{-16} cm^3 $molecule^{-1}$ s^{-1}, respectively, summing to a total rate coefficient of 4.36×10^{-15} cm^3 $molecule^{-1}$ s^{-1} for O_3 + 2,5-DMF, approximately one order of magnitude higher than the experimental values. The calculated rate coefficient for the POZ-OUT pathway is in close agreement with the experimental values reported by Matsumoto (2011) and Illmann and Rösgen (2024), who determined rate coefficients of $(4.2 \pm 0.9) \times 10^{-16}$ and $(3.3 \pm 1.0) \times 10^{-16}$ cm^3 $molecule^{-1}$ s^{-1}, respectively, for the reaction of O_3 with 2,5-DMF. In contrast, the calculated rate coefficient for the POZ-IN pathway, and consequently the total rate coefficient, was found to be approximately one order of magnitude higher than the experimental values. Subsequent POZ decomposition leads to the formation of the Criegee intermediates CI-1 and CI-2, where the POZ-IN yields the Anti-CI conformers, whereas the POZ-OUT yields the Syn-CI conformers. Similar conformer-dependent CI formation has been discussed for sabinene ozonolysis (Wang and Wang, 2017)."
Results section, lines 470–475: "Additional calculations were performed by varying the torsional angle of the Anti-CI-2-forming transition-state geometry to explore the possible formation of Anti-CI-2A, but these calculations also did not establish a definitive formation pathway. Thus, the formation mechanism of Anti-CI-2A remains unresolved in the present study. To assess whether even a small population of Anti-CI-2A could contribute to the experimentally observed O_9 formation, its potential role was further investigated through kinetic sensitivity simulations, as discussed in the following section."

Technical Corrections

REVIEWER COMMENT R1.17

For my own interest, I am curious why the authors use a stochastic solver rather than a traditional ODE solver to handle the kinetic simulations. I would have presumed that the latter was both simpler and more efficient.

RESPONSE

We thank the reviewer for this comment. There was no specific methodological reason for choosing a stochastic solver over a traditional ODE solver. Kinetiscope was selected primarily because we were more familiar with this simulation framework, and it allowed us to conveniently implement the reaction schemes and evaluate the kinetic behavior of the pathways considered in this study. We agree that the reaction system could also be treated using a traditional ODE solver, which may provide a simpler and more computationally efficient approach.

REVIEWER COMMENT R1.18

The species "DICARBO2" is mentioned a few times. It would be helpful to give some form of proper chemical identification of this species when it is first mentioned.

RESPONSE

We thank the reviewer for this suggestion. DICARBO2 is the name Illmann and Rösgen (2024) give to the carbonyl-substituted peroxy radical formed along the Z-CI1 fragmentation pathway in their proposed mechanism (their Scheme 2): fragmentation of Z-CI1 releases CO_2 and a CH_3 radical, leaving a C_4 vinoxy-type radical that adds O_2 to give DICARBO2. Tracking the atoms through that sequence from their stated Z-CI1 formula ($C_6H_8O_4$, matching our own CI/VHP formula convention) gives DICARBO2 = $C_4H_5O_4$. We have added this identification at DICARBO2's first mention in the Introduction.

CHANGES TO MANUSCRIPT

Introduction, lines 85–88: Introduction: "...identified a 1,4-H shift isomerization of the carbonyl-substituted peroxy radical they term DICARBO2 ($C_4H_5O_4$), formed by O_2 addition to the vinoxy-type radical produced when the dominant pathway of the Criegee intermediate (Z-CI1 in their nomenclature) fragments with loss of CO_2 and CH_3 radical, as competitive with bimolecular RO_2 loss..."

REVIEWER COMMENT R1.19

On line 244, the authors refer to "Table 2, Fig. 3". I don't think Table 2 has anything to do with the TME experiments. Perhaps they mean Table 1, or some other Table.

RESPONSE

We agree with the reviewer: Table 2 lists product compositions, not experimental conditions; the TME concentration is given in Table 1. We have corrected the cross-reference in the revised manuscript.

CHANGES TO MANUSCRIPT

Results section, lines 272–273: Results section: "TME addition experiments confirm the contribution of the OH channel...(Table 1; Fig. 3)." (was Table 2).

REVIEWER COMMENT R1.20

On line 267, the phrase "Addition of 100 ppbv NO at delta t = 7 s" makes it sound like NO was added after the reactor had been reacting for 7 s. I doubt that is true and that the NO was part of the initial mixture. I presume the specification of the time was just to indicate which experiment is being considered. Since this description can be confusing it would be good to rephrase it.

RESPONSE

We agree with the reviewer's interpretation: NO was added in the initial reactant mixture for these Δt = 7 s experiments, not added partway through the reaction. We have reworded the sentence in the revised manuscript to remove the ambiguity.

CHANGES TO MANUSCRIPT

Results section, lines 297–298; Table 1: Results section now reads: "NO was introduced into the 2,5-DMF and O_3 reactant mixture at 20, 50, 100, 200, 400, and 500 ppbv, at a residence time of Δt = 7 s, in order to probe the competition between RO_2+NO, autoxidation, and bimolecular RO_2 loss...".

REVIEWER COMMENT R1.21

On p. 17, and p. 22 Fig. ?? needs to be fixed.

RESPONSE

We thank the reviewer for the careful reading. We located and fixed two broken figure references that were displaying as 'Fig. ??': one in the Criegee-intermediate discussion, now resolving to 'Fig. 8a', and one in the kinetic-simulation discussion, now resolving to 'Fig. 9'. All figure cross-references have been re-checked and now resolve correctly.

CHANGES TO MANUSCRIPT

Results section, Sect. 3.4.2, line 400 (previously 'Fig. ??'): "...as shown in Fig. 8 a."
Results section, Sect. 3.4.3, line 493 (previously 'Fig. ??'): "The simulations showed that both O_9 products, $C_6H_7O_9$–c–VIa and $C_6H_7O_9$–c–VIb (Fig. 9), could form, although their formation behavior differed considerably."

REVIEWER COMMENT R1.22

The citation to Castaneda et al. needs to be fixed.

RESPONSE

We thank the reviewer for noting this. The bibliography entry was missing page numbers (placeholder '???–???'). We have added the correct page range (316–324) and issue number, verified against the journal's website (J. Mex. Chem. Soc. 56(3), 2012).

CHANGES TO MANUSCRIPT

Bibliography entry (references.bib): the entry's number and pages fields now read: "number = {3}, pages = {316–324}" (previously missing, rendering as '???–???').

REVIEWER COMMENT R1.23

In the SI, the use of the same label for multiple structures in Figs. S4 and S5, gets a little confusing. Perhaps you could add a, b, c, etc. labels after the numerical labels.

RESPONSE

We thank the reviewer for this suggestion. We have revised the structural labels by adding lowercase letters (a, b, c, etc.) to distinguish different structures sharing the same molecular formula, thereby improving clarity. The corresponding figures, previously numbered S4 and S5, have been renumbered

as Figs. S7 and S8 in the revised Supplementary Information.

CHANGES TO SUPPLEMENT

Figs. S7–S8: revised structural labels and captions are reproduced below.

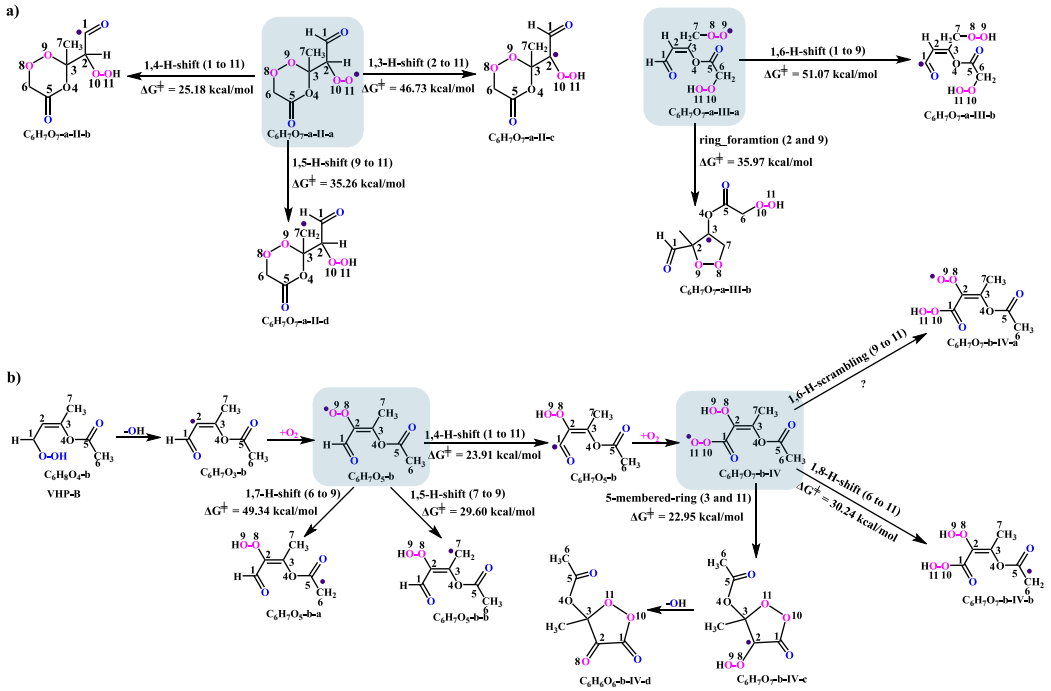


Fig. S7. (a) Additional explored reaction channels for the $C_6H_7O_7$ structures II and III, as defined in the main manuscript. (b) Additional explored reaction channels originating from VHP-B, including 1,x-H shifts (x = 3–8) and ring-closure pathways. Barrier heights ($\Delta G^{\ddagger}$, kcal mol^{-1}) were calculated at the M06-2X/6-31G(d,p) level of theory. A question mark (?) indicates that the corresponding transition state could not be located. Colour code: pink oxygen atoms represent O_2 addition.

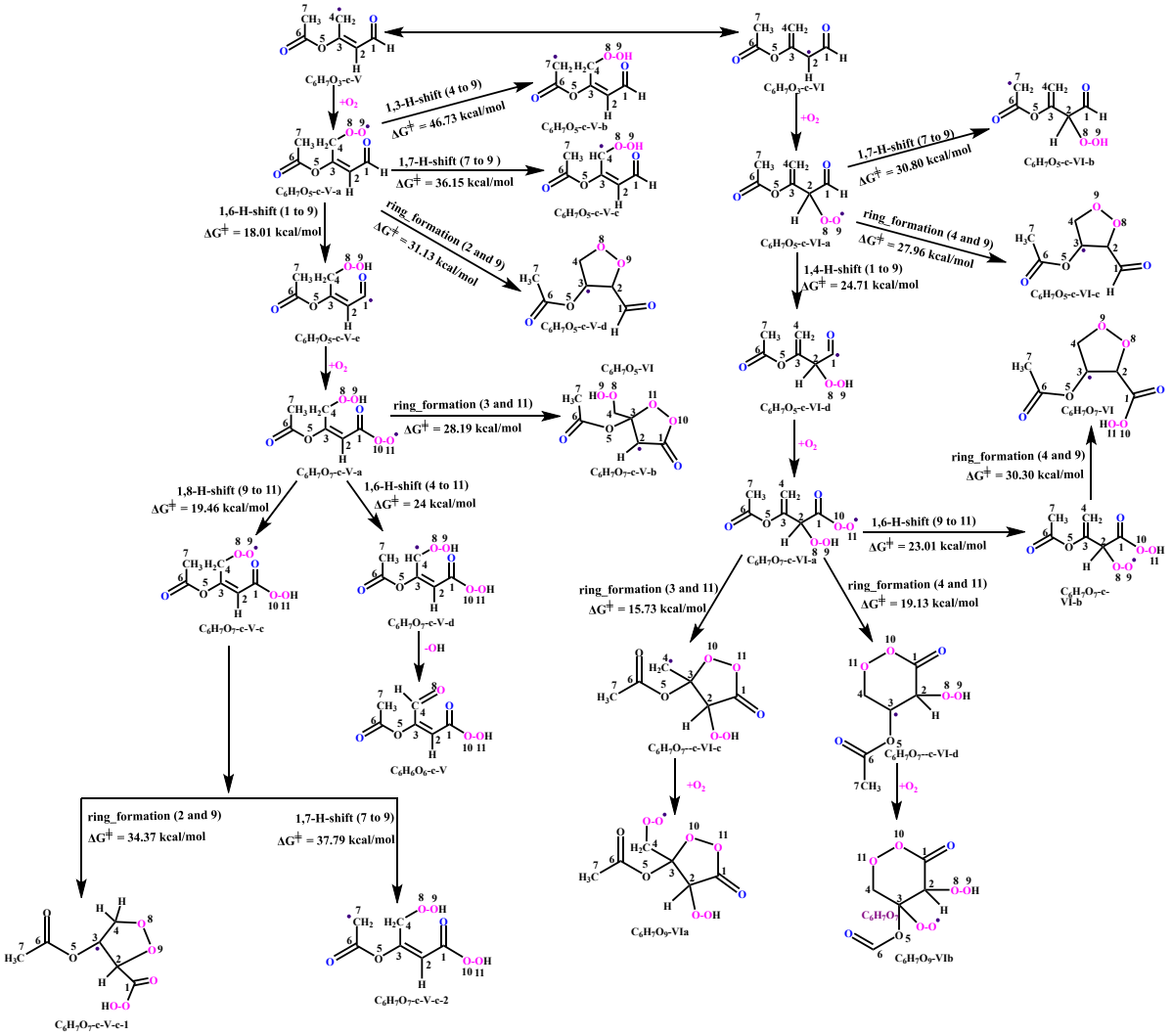


Fig. S8. All explored reaction channels originating from the VHP-C-derived structures V and VI ($C_6H_7O_3$), including 1,x-H shifts (x = 3–8) and ring-closure pathways. Barrier heights ($\Delta G^{\ddagger}$, kcal mol^{-1}) were calculated at the M06-2X/6-31G(d,p) level of theory. Colour code: pink oxygen atoms represent O_2 addition.

REVIEWER COMMENT R1.24

The footnote to Table S3 refers to reaction Scheme 2. Should it instead refer to reaction Scheme 3?

RESPONSE

We thank the reviewer for pointing out this error. The footnote has been corrected to refer to Reaction Scheme 6. Additionally, Table S3 has been renumbered as Table S6 in the revised Supplementary Information.

Referee #2

General comments

Comment 1.)

REVIEWER COMMENT

When I first read the manuscript, I found myself somewhat confused by the way the authors use terms such as “product”, “accretion product” and “HOM monomer”. While “accretion product” is clear, it was not clear to me whether “HOM monomer” is restricted to closed-shell species or whether it also includes the corresponding peroxy radicals. I would therefore encourage the authors to distinguish more clearly between closed-shell products and peroxy radicals, and to explicitly indicate whenever a molecular formula refers to a radical species. I think this would make it much easier for the reader to follow the authors’ reasoning throughout the manuscript.

RESPONSE

We appreciate the reviewer's suggestion to clarify the terminology. We now ground our use of “HOM” explicitly in the criteria of Bianchi et al. (2019), and we distinguish monomeric HOM (the open-shell RO_2 radicals and their closed-shell RO_2+HO_2 termination products) from HOM accretion products. We also name the individual species classes explicitly: RO_2 radicals (which include nearly all of the $C_6H_7O_x$ and $C_6H_9O_x$ series, detected directly by NO_3^- CIMS), closed-shell RO_2+HO_2 termination products (ROOH, $C_6H_{10}O_x$), and RO_2+RO_2 accretion products. Because mass spectrometry alone cannot distinguish isomers, we also note that the same $C_6H_{10}O_x$ formulas are equally consistent with an alcohol/carbonyl pair formed via the Russell RO_2+RO_2 mechanism. This is stated once in Sect. 3.1 and repeated in the footnotes of Tables 2 and 3, and we have gone through Sect. 3.1-3.3 and explicitly named each species as a radical or closed-shell species at its first mention in the text (e.g. ‘the $C_6H_9O_4$ radical’, ‘the $C_6H_7O_7$ and $C_6H_7O_9$ peroxy radicals’, ‘the alkoxy radical RO’). Where a statement applies to the RO_2 radicals specifically, the text now says “HOM peroxy radicals” instead of “HOM monomers”.

CHANGES TO MANUSCRIPT

Results section, lines 211–217, 226–277, 296–347, and 533–542 (passages affected by the terminology revision throughout Sect. 3.1, Sect. 3.3 and the Atmospheric Implications); Abstract, lines 4–14; Table 2 and its footnotes (p. 12):
(1) the definition sentence at the start of Sect. 3.1 now reads “Following the criteria of Bianchi et al. (2019), we refer to the RO_2 radicals of the autoxidation chain and their reaction products collectively as HOM, distinguishing monomeric HOM – the RO_2 radicals and their closed-shell RO_2+HO_2 termination products (ROOH, $C_6H_{10}O_x$) – from HOM accretion products formed by RO_2+RO_2 recombination (Table 2). The same nominal formulas ($C_6H_{10}O_x$) are equally consistent with an alcohol/carbonyl pair from the Russell RO_2+RO_2 mechanism.”
(2) explicit radical/closed-shell wording added at each species’ first mention throughout Sect. 3.1 and Sect. 3.3 (e.g. the $C_6H_9O_4$ radical, the $C_6H_7O_7$ and $C_6H_7O_9$ peroxy radicals, the alkoxy radical RO).
(3) “HOM monomer(s)” replaced by “HOM peroxy radical(s)” where the RO_2 radical is meant (Sect. 3.1, 3.3, 3.4 and Conclusions) and by “HOM” in the Abstract. In the Atmospheric Implications, “monomeric HOM” is retained as the umbrella term (RO_2 radicals plus their closed-shell termination products), as defined in Sect. 3.1. Table 2 (and, correspondingly, Table 3): the peroxy-radical rows are now labelled RO_2 instead of HOM O_n, since HOM is used as the umbrella term; the footnotes define RO_2 as a peroxy radical; Fragment as a radical formed via fragmentation of the C_6 skeleton; ROOH as a closed-shell RO_2+HO_2 termination product (the same nominal formula is equally consistent with an alcohol/carbonyl pair from the Russell mechanism); and Accretion as an RO_2+RO_2 recombination product.

Table 2. Chemical compositions and $[MNO_3^-]$ adduct m/z values of oxidation products observed from 2,5-DMF ozonolysis and OH-initiated oxidation, classified by carbon skeleton and oxygenation class.

O_3-derived products			OH-derived products		
Type	Formula	m/z (Th)	Type	Formula	m/z (Th)
Intermediate[a]	$C_6H_8O_4$	206.0306	RO_2	$C_6H_9O_6$	239.0280
Fragment	$C_4H_3O_6$	208.9813	ROOH	$C_6H_{10}O_6$	240.0359
Fragment	$C_4H_5O_6$	210.9970	Fragment	$C_5H_7O_7$	241.0073
Fragment	$C_4H_6O_6$	212.0048	RO_2	$C_6H_9O_8$	271.0178
Fragment	$C_4H_5O_7$	226.9918	ROOH	$C_6H_{10}O_8$	272.0256
RO_2	$C_6H_7O_6$	237.0124	Accretion	$C_{10}H_{14}O_6$	292.0671
RO_2	$C_6H_7O_7$	253.0082	Accretion	$C_{10}H_{12}O_8$	322.0412
RO_2	$C_6H_7O_8$	269.0022	Accretion	$C_{10}H_{14}O_9$	340.0512
RO_2	$C_6H_7O_9$	284.9971	Accretion	$C_{12}H_{18}O_8$	352.0876
			Accretion	$C_{11}H_{16}O_9$	354.0669

m/z values correspond to $[MNO_3^-]$ adduct ions; neutral molecular compositions are listed. [a] Primary ozonide (POZ) and its Criegee intermediate decomposition products prior to OH loss. RO_2: peroxy radical. ROOH: closed-shell $RO_2 + HO_2$ termination product; the same nominal formula is equally consistent with an alcohol/carbonyl pair from the Russell $RO_2 + RO_2$ mechanism. Accretion: bimolecular $RO_2 + RO_2$ recombination product. Fragment: radical formed via fragmentation of the C_6 skeleton.

Comment 2.)

REVIEWER COMMENT

The discussion of the experimental results addresses the competition between unimolecular and bimolecular radical reactions and the shift in product distribution with increasing reaction time. This is associated with a larger contribution of OH chemistry and higher RO_2 concentrations. Regarding this discussion, I have two questions that might be worth addressing.

a) Do the authors have an estimate of the peroxy radical concentrations in their experimental set-up, perhaps based on the kinetic modelling they performed for POZ formation and decomposition? If not, would it be possible to estimate radical concentrations in the flow tube? As a reader I would be curious to know at least a rough estimate of the RO_2 concentration and how they change under the different experimental conditions, since RO_2 concentrations are used to explain the change in product distribution.

b) The authors have varied initial reactant concentrations by more than a factor of ten in the "O_3 only" and "O_3 + TME" experiments. If the longer reaction time leads to a clear change in product distribution due to higher RO_2 concentrations, should a similar effect not also be observed when varying the initial reactant concentrations over such a large range? It might therefore be worth providing more details on how the product distribution changes as a function of the initial reactant concentration.

RESPONSE

We thank the reviewer for these questions. We agree that both the initial precursor concentrations and residence time should be considered when interpreting the observed changes in product distribution.

a) To address the first question, we performed additional kinetic simulations separately for the O_3-only and O_3+TME experimental conditions, using the corresponding initial precursor concentrations and residence times. The complete reaction schemes and time-averaged concentrations are provided in the revised Supplementary Information (Sect. S6.3, Reaction Schemes 3–4, and Tables S3–S4).

The simulations showed higher concentrations of several RO_2 intermediates under the 7 s conditions.

For example, $\mathrm{VHP-B_O7}$ increased from 2.13×10^7 to 1.42×10^9 molecules cm^{-3} (Table S4), while the OH-derived O_6 RO_2 intermediate $\mathrm{BPR_OH_OO_S_O6}$ increased from 3.36×10^7 to 5.34×10^7 molecules cm^{-3} (Table S3). Not all intermediates increased, reflecting the balance between their formation and subsequent consumption. Furthermore, the modeled bimolecular product $\mathrm{sink_1}$ increased from 3.93×10^7 to 5.01×10^8 molecules cm^{-3}, while $\mathrm{sink_3}$ and $\mathrm{sink_8}$ showed nonzero concentrations only under the 7 s conditions. These results are consistent with additional RO_2 processing, including bimolecular reactions, under the longer-residence-time conditions.

b) Regarding the second question, we examined the experimental HOM peroxy radical signal distribution at fixed residence time. Here the ratio refers to the open-shell RO_2 radicals only (OH-derived $C_6H_9O_6$ and $C_6H_9O_8$ relative to ozonolysis-derived $C_6H_7O_{6–9}$); closed-shell products are not included. The ratio of OH-derived to ozonolysis-derived peroxy radical signals decreased with increasing initial precursor concentrations at both residence times: at $\Delta t = 7\,\mathrm{s}$, the ratio decreased from 47.5 to 9.0 to 6.1 across the three 2,5-DMF mixing ratios of 85, 169, and 254 ppbv, respectively, while at $\Delta t = 0.8\,\mathrm{s}$, it decreased from 39.9 to 8.7 as the 2,5-DMF mixing ratio increased from 628 to 1046 ppbv. The decrease reflects the ozonolysis-derived radical signals growing faster than the OH-derived ones as the precursor loading increases (the ratios were recomputed directly from the normalized spectra and reproduce the quoted values). Thus, increasing precursor loading did not reproduce an increase in the relative contribution of OH-derived peroxy radical signals observed at the longer residence time.

We further examined how the product distribution depends on the initial 2,5-DMF mixing ratio at a fixed residence time of $\Delta t = 7\,\mathrm{s}$. The ratio of the summed closed-shell termination product signals ($C_6H_{10}O_6$ and $C_6H_{10}O_8$) to the corresponding HOM peroxy radical signals ($C_6H_9O_6$ and $C_6H_9O_8$) increased with increasing precursor loading in both the O_3-only and O_3+TME experiments; in the O_3-only series it rose from 0.014 to 0.107 to 0.200 across the three 2,5-DMF mixing ratios of approximately 85, 169, and 254 ppbv, respectively. Accretion product signals also became more prominent at higher precursor loading, although several accretion species were close to or below the detection threshold at the lowest concentration, so this trend is reported only qualitatively. The increasing termination-to-radical signal ratio indicates a greater relative abundance of closed-shell termination products at higher precursor loading, consistent with an increased contribution from bimolecular RO_2 termination, either RO_2+HO_2 (yielding ROOH) or the Russell RO_2+RO_2 channel (yielding an alcohol and a carbonyl), which have the same nominal composition and cannot be distinguished by mass spectrometry alone. However, because of compound-dependent NO_3^- sensitivity, these signal ratios do not provide direct quantitative measures of reaction branching fractions or RO_2 concentrations.

Together, the experimental observations and kinetic simulations suggest that the time available for subsequent oxidation chemistry may contribute to the observed product distribution. However, because the initial precursor concentrations also differed between the two experimental conditions, their individual effects cannot be fully separated. We have therefore revised the manuscript discussion to acknowledge both factors, rather than attributing the changes exclusively to residence time or higher RO_2 concentrations. We have added the estimated RO_2 concentrations and the corresponding kinetic-model details to the Supporting Information.

CHANGES TO MANUSCRIPT

Results section, lines 245–251: “The prominent closed-shell products $C_6H_{10}O_6$ and $C_6H_{10}O_8$ indicate a contribution from bimolecular termination at $\Delta t = 7\,\mathrm{s}$. These formulas are consistent with RO_2 + HO_2 termination (ROOH); however, mass spectrometry alone cannot distinguish isomeric structures, and an alcohol/carbonyl pair formed via the Russell RO_2 + RO_2 self- or cross-reaction (Russell, 1957) remains an equally plausible contributor to the same nominal composition. Kinetic simulations of the OH-initiated channel likewise show

higher time-averaged RO_2 intermediate concentrations under the 7 s conditions (Sect. S6.3, Table S3). Because the initial 2,5-DMF and O_3 concentrations also differed between the 0.8 and 7 s experiments, these differences cannot be attributed to residence time alone." The concentration-series analysis (OH:O_3 product ratio and closed-shell-termination:peroxy-radical signal ratio vs. initial [2,5-DMF]) is reported in this response letter.

CHANGES TO SUPPLEMENT

Sect. S6.3, Reaction Schemes 3–4 and Tables S3–S4: kinetic-model RO_2 concentration estimates (by species) for the O_3-only and O_3+TME experiments at 0.8 and 7 s, reproduced below.

Table S3. Time-averaged concentrations of RO_2 intermediates and bimolecular RO_2 reaction products obtained from Reaction Scheme 3 at 0.8 and 7 s under the corresponding O_3 + TME experimental conditions.

Species	**Average concentration (molecules cm^{-3})**	
	0.8 s	**7 s**
add_2_5_O4	2.04×10^9	2.43×10^9
add_3_4_O4	6.12×10^4	1.30×10^4
abs_O4	4.72×10^6	6.80×10^6
BPR_OH_OO_S_O6	3.36×10^7	5.34×10^7
BPR_OH_OO_S_O6_an	3.87×10^5	1.32×10^6
BPR_OH_OO_O_O6	0	0
BPR_OH_OO_O_O6_an	0	0
TME_RO2	2.90×10^7	1.58×10^8
Bimolecular RO_2 reaction products		
sink_1	3.93×10^7	5.01×10^8
sink_3	0	8.41×10^5
sink_8	0	1.27×10^6

The labels add_2_5_O4 and add_3_4_O4 represent RO_2 species formed following OH addition at the 2,5- and 3,4-positions of 2,5-DMF, respectively, while abs_O4 represents the RO_2 species formed following H-atom abstraction from a methyl group. The species BPR_OH_OO_S_O6 and BPR_OH_OO_S_O6_an correspond to $C_6H_9O_6$-Ia and $C_6H_9O_6$-Ib, respectively, whereas BPR_OH_OO_O_O6 and BPR_OH_OO_O_O6_an correspond to $C_6H_9O_6$-IIa and $C_6H_9O_6$-IIb, respectively. The labels sink_1, sink_3, and sink_8 represent products of the bimolecular RO_2 + RO_2 reactions included in Reaction Scheme 3. Specifically, sink_1 corresponds to the self-reaction of add_2_5_O4, whereas sink_3 and sink_8 correspond to the cross-reaction between add_2_5_O4 and abs_O4, written in opposite reactant orders in the reaction scheme. These sink species represent modeled bimolecular reaction products rather than RO_2 intermediates.

Table S4. Time-averaged O_7 RO_2 concentrations obtained from Reaction Scheme 4 at 0.8 and 7 s using 1×10^8 particles and a random number seed of 28224.

Species	Model Input (molecule cm^{-3})	Model Output Average concentration (molecule cm^{-3})
Reaction time: 0.8 s		
VHP-A_O7	–	0
VHP-A_rg_6_O7	–	0
VHP-A_rg_7_O7	–	0
VHP-B_O7	–	2.13×10^7
Reaction time: 7 s		
VHP-A_O7	–	0
VHP-A_rg_6_O7	–	0
VHP-A_rg_7_O7	–	0
VHP-B_O7	–	1.42×10^9

Comment 3.)

REVIEWER COMMENT

I would encourage the authors to address the impact of NO on HOM formation more thoroughly, based on the following comments and questions:

Comment 3.a)

REVIEWER COMMENT

Table 1 states that the NO mixing ratios were varied in the range of 20–500 ppbv in these experiments, but only results obtained at 100 ppbv are presented. Is there a specific reason for choosing this condition, or were the results largely independent of the NO mixing ratio?

RESPONSE

We thank the reviewer for the question. 100 ppbv was chosen as the reference condition because it is the highest NO level at which every assigned organonitrate product remains above the detection limit: the dose-response of all nine organonitrate species across the full 20-500 ppbv series (Fig. S4) shows that the organonitrate formation pathway is not yet fully established at 20-50 ppbv, is essentially complete by 100 ppbv, and partially recedes above 100 ppbv, with the higher-generation products ($C_6H_9O_8NO$, $C_6H_9O_9NO$) falling below the detection limit at 200 ppbv and above. The time-resolved signal at 100 ppbv (Fig. S5) confirms the formation pathway is already fully developed within the 7 s residence time.

CHANGES TO MANUSCRIPT

Results section, lines 299–301: "Of this series, the 100 ppbv NO spectrum (Fig. 5) is used as the reference, as it represents the highest NO level at which all assigned organonitrate products, including the least intense ones, remain above the detection limit."

CHANGES TO SUPPLEMENT

Sect. S4, lines 43–47 and Figs. S4–S5: "The full NO concentration series underlying Sect. 3.3 of the main text is given here (conditions given in Table 1 of the main text)." The dose-response and time-resolved measurements

are reproduced below.

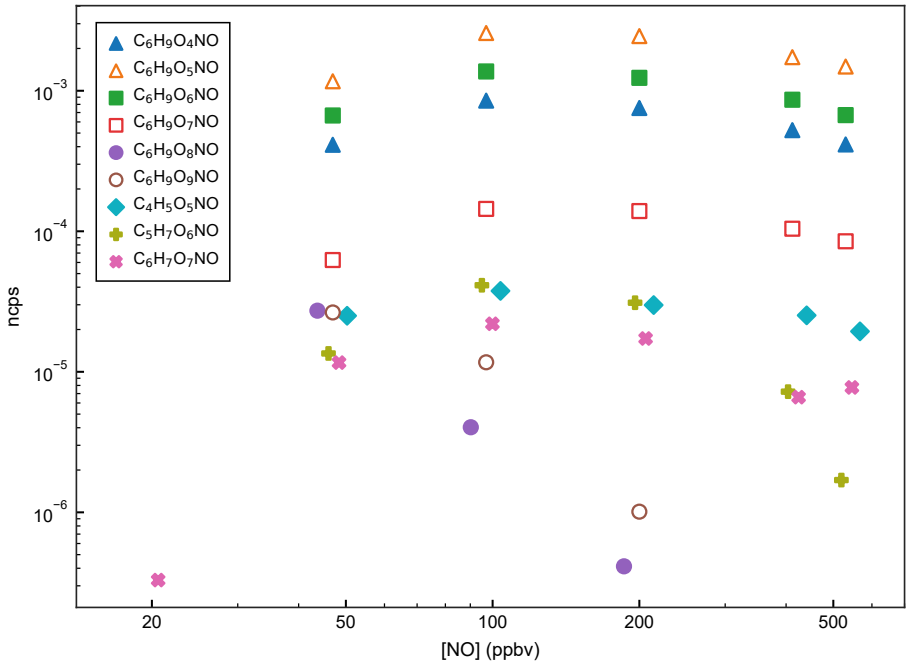


Fig. S4. NO dose-response (normalized counts s^{-1}, log scale) of the nine assigned organonitrate species at $\Delta t = 7$ s. Filled markers: direct $RO_2 + NO$ termination products ($C_6H_9O_4NO$, $C_6H_9O_6NO$, $C_6H_9O_8NO$, $C_6H_7O_7NO$). Open markers: alkoxy-mediated products ($C_6H_9O_5NO$, $C_6H_9O_7NO$, $C_6H_9O_9NO$), formed via an additional $RO_2 + NO \rightarrow RO + NO_2$ / H-shift / O_2-addition cycle before the second $RO_2 + NO$ termination step. $C_6H_7O_7NO$ is the direct, ozonolysis-channel product of its own parent $C_6H_7O_7$ (RO_2, per Tables 2 and 3), and is the only one of the nine species detected at 20 ppbv NO (near the detection floor); the remaining eight are not observed until 50 ppbv. $C_4H_5O_5NO$ and $C_5H_7O_6NO$ are organonitrates of fragment radicals and are shown filled by default; the direct/alkoxy-mediated distinction does not apply to them.

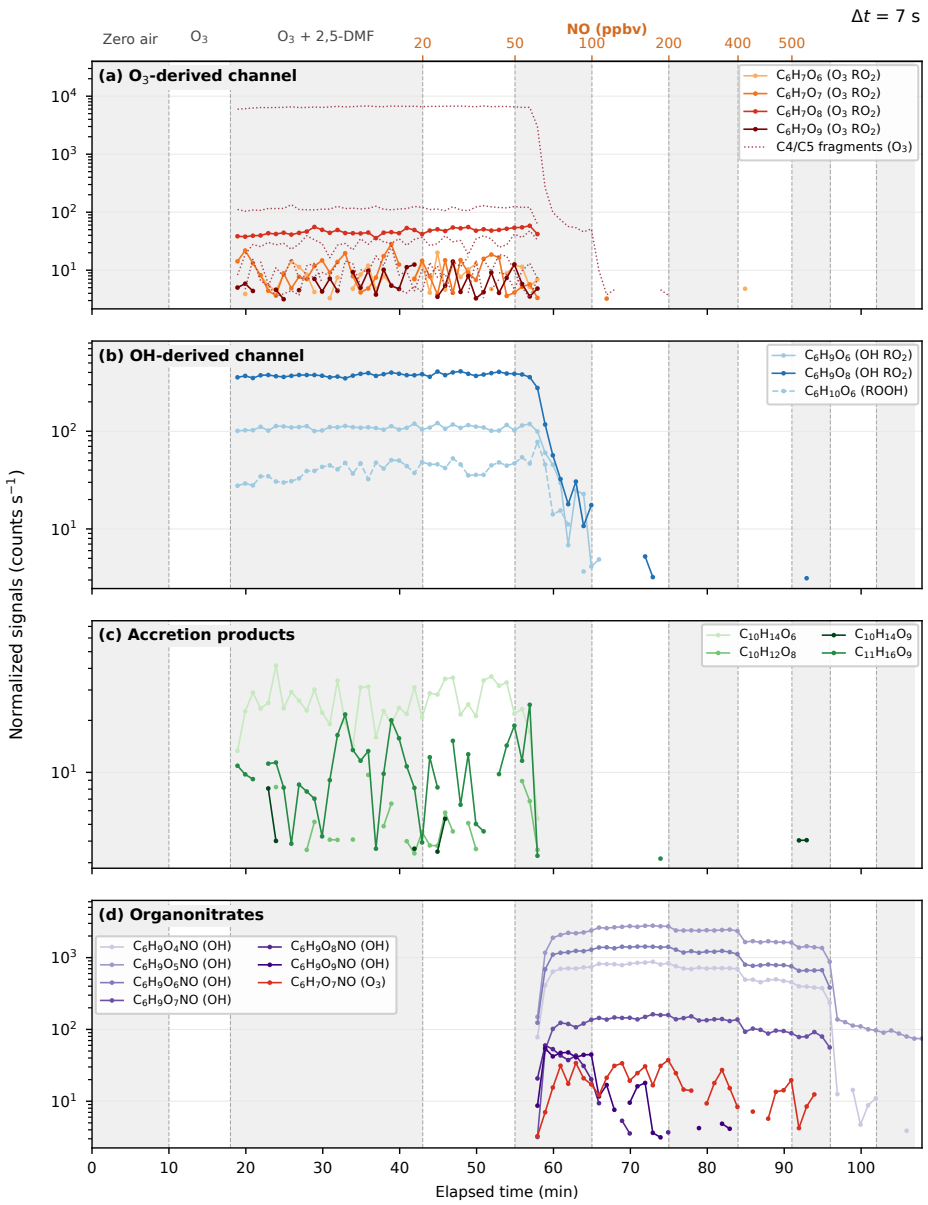


Fig. S5. Time-resolved NO_3^- CIMS signal (normalized counts s^{-1}) of the O_3-derived, OH-derived, accretion, and organonitrate product families during the 2,5-DMF + O_3 + NO experiment at $\Delta t = 7$ s, spanning the full 0–500 ppbv NO series: (a) O_3-derived channel, (b) OH-derived channel, (c) accretion products, (d) organonitrates. Shaded/unshaded bands mark successive experimental phases (zero air, O_3, O_3 + 2,5-DMF, and each NO step, labelled along the top axis).

Comment 3.b)

REVIEWER COMMENT

Did the authors perform any kinetic modelling to assess the relative contributions of 2,5-DMF ozonolysis and the reaction of 2,5-DMF with OH under these experimental conditions? I am wondering whether, based on the information provided in Table 1, the O_3 loss is dominated (by about 95%, if I am not mistaken) by its reaction with NO. In this context, can the authors rule out that NO_3 formation and subsequent reaction of 2,5-DMF with NO_3, which proceeds close to the collision limit, play a role and potentially interfere with the organic nitrate formation monitored here? I am not questioning the experimental results, but I think this point would be worth addressing.

RESPONSE

We thank the reviewer for this question; kinetic simulations (Kinetiscope, Reaction Scheme 2, SI Sect. S6.2) address both parts of it. On the relative rate of O_3 loss to NO versus to 2,5-DMF: using $k(\mathrm{NO} + \mathrm{O_3}) = 1.70 \times 10^{-14}$ cm^3 molecule^{-1} s^{-1} and $k(2,5\text{-DMF} + \mathrm{O_3}) = 4.36 \times 10^{-15}$ cm^3 molecule^{-1} s^{-1} together with the experimental concentrations in Table 1, the initial rate of O_3 consumption via reaction with NO is approximately 2.3 times that via reaction with 2,5-DMF at the 100 ppbv reference condition – lower than the reviewer's ∼95% estimate, since this is an initial-rate ratio rather than a cumulative loss fraction and NO itself is consumed as the reaction proceeds. On the NO_3-interference sub-question: NO_3 forms in situ via NO + O_3 → NO_2 + O_2 followed by the much slower NO_2 + O_3 → NO_3 + O_2 step ($k = 3.2 \times 10^{-17}$ cm^3 molecule^{-1} s^{-1}, roughly three orders of magnitude slower than O_3+NO), which limits NO_3 accumulation over the 7 s residence time even though NO_3 itself reacts rapidly with 2,5-DMF ($k = 1.02 \times 10^{-10}$ cm^3 molecule^{-1} s^{-1}, Newland et al., 2022). Averaged over five independent Kinetiscope runs with different random-number seeds, the branching contribution of 2,5-DMF+NO_3 is $(0.013 \pm 0.007)\,\%$ relative to the combined 2,5-DMF+O_3 and 2,5-DMF+NO_3 reactions. This uses a simplified NO_x scheme and is not a complete quantitative description of the system, but it indicates NO_3-initiated chemistry is a minor contributor, so the organonitrate products discussed in Sect. 3.3 predominantly arise from RO_2+NO chemistry rather than NO_3-initiated chemistry.

CHANGES TO MANUSCRIPT

Results section, Sect. 3.3, lines 301–316: "As NO_3 can also form in situ through the reaction of NO_2 with O_3 under the RO_2 + NO experimental conditions, we assessed its potential contribution to the observed organonitrate products. For this purpose, kinetic simulations were performed using Kinetiscope, as described in detail in Sect. S6.2, using Reaction Scheme 2. The rate coefficient for the reaction of O_3 with NO ($k = 1.70 \times 10^{-14}$ cm^3 molecule^{-1} s^{-1}) is approximately four times higher than that for O_3 with 2,5-DMF ($k = 4.36 \times 10^{-15}$ cm^3 molecule^{-1} s^{-1}). Considering the corresponding experimental concentrations, the initial rate of O_3 consumption through its reaction with NO is approximately 2.3 times higher than that through its reaction with 2,5-DMF. The kinetic simulations, performed using the corresponding experimental concentrations, showed that although NO_3 formed through the NO + O_3 → NO_2 + O_2 and subsequent NO_2 + O_3 → NO_3 + O_2 reactions can react rapidly with 2,5-DMF ($k = 1.02 \times 10^{-10}$ cm^3 molecule^{-1} s^{-1}), NO_3 formation from NO_2 + O_3 is itself slow ($k = 3.2 \times 10^{-17}$ cm^3 molecule^{-1} s^{-1}, roughly three orders of magnitude slower than O_3 + NO), limiting NO_3 accumulation within the 7 s residence time. Five independent simulations were performed using different random-number seeds, and the contribution of the 2,5-DMF + NO_3 reaction was consistently low, with an average branching contribution of $(0.013 \pm 0.007)\,\%$ relative to the combined 2,5-DMF + O_3 and 2,5-DMF + NO_3 reactions (Sect. S6.2 Table S2). This estimate uses a simplified NO_x scheme and is not intended as a complete quantitative description of the system, but it indicates that NO_3-initiated chemistry is a minor contributor under these conditions. We therefore suggest that the organonitrate products discussed below should predominantly arise from RO_2 + NO chemistry rather than NO_3-initiated chemistry."

CHANGES TO SUPPLEMENT

Sect. S6.2: new Table S2 (average product concentrations from Kinetiscope simulations of 2,5-DMF oxidation by O_3 and NO_3 over a 7 s period using five random-number seeds, and the resulting NO_3 contribution), reproduced below.

Table S2. Average product concentrations obtained from Kinetiscope simulations of 2,5-DMF oxidation by O_3 and NO_3 over a 7 s simulation period using five different random-number seeds. The relative contribution of the NO_3-initiated pathway was calculated from the average concentrations of DMF_NO3, POZ-IN, and POZ-OUT.

Random-number seed	Average concentration (molecules cm^{-3})			NO_3 contribution (%)
	POZ-IN	POZ-OUT	DMF_NO3	
28224	6.219×10^{10}	5.215×10^{9}	4.082×10^{5}	0.000606
11752	6.215×10^{10}	5.222×10^{9}	9.495×10^{6}	0.014091
26138	6.218×10^{10}	5.202×10^{9}	1.068×10^{7}	0.015847
11284	6.208×10^{10}	5.203×10^{9}	1.068×10^{7}	0.015870
21542	6.223×10^{10}	5.229×10^{9}	1.139×10^{7}	0.016876
			Mean ± standard deviation	0.013 ± 0.007

Comment 3.c)

REVIEWER COMMENT

The authors state that the $RONO_2$ species observed in the mass spectra are $C_6H_9O_{4–9}NO$ and $C_6H_7O_7NO$ and assign these species to the different peroxy radicals formed in the system. However, I do not think that this assignment is entirely correct. If the dominant peroxy radicals formed are $C_6H_9O_4$ following OH addition, and $C_6H_9O_6$ and $C_6H_9O_8$ following successive unimolecular isomerization, the corresponding $RONO_2$ species should be $C_6H_9O_4NO$, $C_6H_9O_6NO$, and $C_6H_9O_8NO$. In contrast, organic nitrates of the form $C_6H_9O_XNO$, where X is an odd number, would require an intermediate alkoxy radical step.

RESPONSE

We agree with the reviewer's distinction and have revised the paragraph to make the assignments explicit. $C_6H_9O_4NO$, $C_6H_9O_6NO$, and $C_6H_9O_8NO$ are assigned as direct RO_2+NO termination products of the three successive RO_2 generations formed by unimolecular H-shift/O_2-addition ($C_6H_9O_4$ → $C_6H_9O_6$ → $C_6H_9O_8$), while the odd-oxygen members ($C_6H_9O_5NO$, $C_6H_9O_7NO$, $C_6H_9O_9NO$) require an intermediate alkoxy-radical step: a first RO_2+NO reaction forms RO, which isomerizes via H-shift/O_2-addition to a more oxygenated RO_2, which is then terminated by a second RO_2+NO reaction. $C_5H_7O_6NO$ and $C_4H_5O_5NO$, organonitrates of fragment radicals, lend further support to this alkoxy branch, since carbon-skeleton loss requires an RO intermediate.

CHANGES TO MANUSCRIPT

Results section, lines 317–319: "The even-oxygen members ($C_6H_9O_4NO$, $C_6H_9O_6NO$, $C_6H_9O_8NO$) are direct RO_2 + NO termination products of the successive unimolecular RO_2 generations, while the odd-oxygen members ($C_6H_9O_5NO$, $C_6H_9O_7NO$, $C_6H_9O_9NO$) require an intermediate alkoxy-radical step, as detailed below." The subsequent explanation, at lines 319–329, reads: "The OH-initiated RO_2 chain established in Sect. 3.1 ($C_6H_9O_4$ → $C_6H_9O_6$ → $C_6H_9O_8$, with each generation separated by an H-shift/O_2-addition step) directly sets the RO_2 + NO termination products: a single bimolecular step converts each generation into its corresponding organonitrate, giving $C_6H_9O_4NO$, $C_6H_9O_6NO$, and $C_6H_9O_8NO$. The odd-oxygen members ($C_6H_9O_5NO$, $C_6H_9O_7NO$, and $C_6H_9O_9NO$), in contrast, require an alkoxy-radical intermediate: RO_2 + NO first produces RO (i.e., one oxygen fewer than the parent RO_2), which then undergoes H-shift and O_2 addition to regenerate a more oxygenated RO_2, and a second RO_2 + NO reaction subsequently yields the observed organonitrate. $C_5H_7O_6NO$ and $C_4H_5O_5NO$, organonitrates of fragment radicals, lend further support to this alkoxy branch, since, as established in Sect. 3.1, carbon-skeleton loss requires an alkoxy-radical intermediate, and their detection thus confirms that RO_2 + NO indeed generates RO under the present conditions. An ozonolysis-derived organonitrate, $C_6H_7O_7NO$, is also detected; because the ozonolysis-channel RO_2 chain

proceeds through odd-oxygen generations ($C_6H_7O_5 \rightarrow C_6H_7O_7$, Sect. 3.1), $C_6H_7O_7NO$ is simply a direct termination product of the $C_6H_7O_7$ radical."

Comment 3.d)

REVIEWER COMMENT

The authors initially state and later conclude that 100 ppbv NO suppresses autoxidation. However, this appears to be inconsistent with the results presented. If I understand the proposed reaction mechanism correctly, all $RONO_2$ species except $C_6H_9O_4NO$ are formed following unimolecular isomerization. Could the authors clarify how these results support the conclusion that 100 ppbv NO suppresses autoxidation?

RESPONSE

We thank the reviewer for pointing out this inconsistency and agree with their reading of the results. NO does not suppress the unimolecular isomerization step itself. The H-shift/O_2-addition sequence remains unimolecular and independent of [NO], and every organonitrate generation, including the later, isomerization-dependent ones, is detectable at 100 ppbv. Instead, 100 ppbv NO outcompetes the subsequent bimolecular RO_2+RO_2/RO_2+HO_2 steps at every generation, intercepting the RO_2 population before it can react further with RO_2 or HO_2. This is why the HOM monomers, closed-shell termination products, and accretion products those steps would otherwise produce all fall below the detection limit, while the organonitrate series remains fully populated. We have removed the "suppresses autoxidation" language and replaced it with this bimolecular-interception framing in Sect. 3.3 and in the Atmospheric Implications section.

CHANGES TO MANUSCRIPT

Results section, lines 343–347 ("...the unimolecular H-shift/O_2-addition isomerization proceeds unperturbed at 100 ppbv NO; what NO changes is only the bimolecular fate of the resulting RO_2 pool. At 100 ppbv, RO_2 + NO is already fast enough to intercept the radical population before it can react further with RO_2 or HO_2, and does so increasingly completely at each successive generation, which is why the ROOH and accretion products otherwise formed in the NO-free system are absent here.").
Atmospheric Implications section, lines 537–542 ("In combustion plumes containing sufficient NO, RO_2 + NO competes with further autoxidation and with RO_2 + RO_2 and RO_2 + HO_2 reactions. In our experiments, NO addition shifted the product distribution toward organonitrates and reduced the signals of non-nitrated HOM monomers and accretion products. As NO concentrations decrease during plume ageing, reduced interception by NO may allow further autoxidation, depending on the competing radical sinks. Both organonitrates and non-nitrated oxidation products may contribute to SOA growth if their volatility permits condensation onto existing particles.")
The supporting NO-series measurements are reproduced on response pp. 29–30.

Comment 4.)

REVIEWER COMMENT

The authors performed calculations indicating a strong preference for Syn-CI-2 formation (about 95%) among the Syn conformers, as also shown in Fig. 7. This is an interesting result, but I find it difficult to assess its overall significance without any information on the Anti conformers and, consequently, on the relative importance of all possible conformers. This seems particularly important because, in Fig. 6, the authors highlight that key intermediates leading to HOM formation originate from Syn-CI-1 and Anti-CI-2, for which the branching fraction is either low (Syn-CI-1) or not provided (Anti-CI-2).

If possible, can the authors comment on the relative importance of all CI conformers?

RESPONSE

We thank the reviewer for this comment. We agree that the branching fractions reported in the original manuscript, approximately 5 % for Syn-CI-1 and 95 % for Syn-CI-2, considered only the Syn-CI-forming pathways and therefore did not provide a complete description of the relative importance of all four CI conformers.
Prompted by this comment and a related question from Reviewer 1, we further investigated the POZ decomposition pathways and identified the corresponding transition states leading to both Syn- and Anti-CI conformers. In the revised calculations, we have therefore included the formation pathways of all four CI conformers and evaluated their branching fractions using master-equation calculations. At 298 K and 1 atm, the calculated branching fractions are 0.69 % for Syn-CI-1, 7.00 % for Syn-CI-2, 2.83 % for Anti-CI-1, and 89.48 % for Anti-CI-2. These results indicate that Anti-CI-2 is the dominant conformer formed during POZ decomposition, whereas Syn-CI-1 represents a minor channel.
We have updated the manuscript and corresponding figures to include the revised branching fractions and to clarify the relative importance of all four CI conformers.

CHANGES TO MANUSCRIPT

Results section, lines 361–375: "In the present study, two distinct orientations of O_3 addition to 2,5-DMF were investigated, leading to the formation of primary ozonides denoted as POZ-IN and POZ-OUT, with calculated rate coefficients of 4.02×10^{-15} and 3.37×10^{-16} cm^3 $molecule^{-1}$ s^{-1}, respectively, summing to a total rate coefficient of 4.36×10^{-15} cm^3 $molecule^{-1}$ s^{-1} for O_3 + 2,5-DMF, approximately one order of magnitude higher than the experimental values. The calculated rate coefficient for the POZ-OUT pathway is in close agreement with the experimental values reported by Matsumoto (2011) and Illmann and Rösgen (2024), who determined rate coefficients of $(4.2 \pm 0.9) \times 10^{-16}$ and $(3.3 \pm 1.0) \times 10^{-16}$ cm^3 $molecule^{-1}$ s^{-1}, respectively, for the reaction of O_3 with 2,5-DMF. In contrast, the calculated rate coefficient for the POZ-IN pathway, and consequently the total rate coefficient, was found to be approximately one order of magnitude higher than the experimental values. Subsequent POZ decomposition leads to the formation of the Criegee intermediates CI-1 and CI-2, where the POZ-IN yields the Anti-CI conformers, whereas the POZ-OUT yields the Syn-CI conformers. Similar conformer-dependent CI formation has been discussed for sabinene ozonolysis (Wang and Wang, 2017). Syn-CI-1 lies approximately 13 kcal mol^{-1} higher in energy than Syn-CI-2, while Anti-CI-1 is approximately 11 kcal mol^{-1} higher in energy than Anti-CI-2, as illustrated by the potential energy surface in Fig. 7. The branching fractions for chemically activated POZ decomposition leading to Syn-CI-1, Anti-CI-1, Syn-CI-2, and Anti-CI-2 were calculated using MESMER and found to be 0.69 %, 2.83 %, 7.00 %, and 89.48 %, respectively, indicating that the formation of Anti-CI-2 is the dominant decomposition channel."

Comment 5.)

REVIEWER COMMENT

The authors show that the dioxirane route appears to be the dominant loss pathway for the Syn-CI-1 conformer, although a 1,4-H shift is accessible. This is unusual and rather surprising. Nevertheless, the authors highlight the VHP formed via the 1,4-H shift as a key intermediate in Fig. 6. I assume this is because the VHP is a key intermediate in HOM formation, irrespective of the relative importance of this pathway? If this is the case, I would encourage the authors to clarify this point in the figure caption.

RESPONSE

We thank the reviewer for this comment. We agree that highlighting VHP-A as a key intermediate

could incorrectly imply that its formation represents a dominant reaction channel. This was not our intention. VHP-A was highlighted because it provides a mechanistic connection between the Syn-CI-1 pathway and the subsequent reaction sequence leading toward HOM formation, rather than because it represents a major branching channel.

As indicated by our calculations, dioxirane formation is the dominant loss pathway for Syn-CI-1, whereas the competing 1,4-H shift leading to VHP-A represents a minor channel. We have therefore revised the figure caption to clarify that the intermediates highlighted in red are those undergoing subsequent reaction steps toward HOM formation, rather than necessarily representing the dominant reaction pathways.

CHANGES TO MANUSCRIPT

Fig. 6 caption: revised as reproduced below ("Red highlights intermediates that undergo subsequent reaction steps leading toward HOM formation").

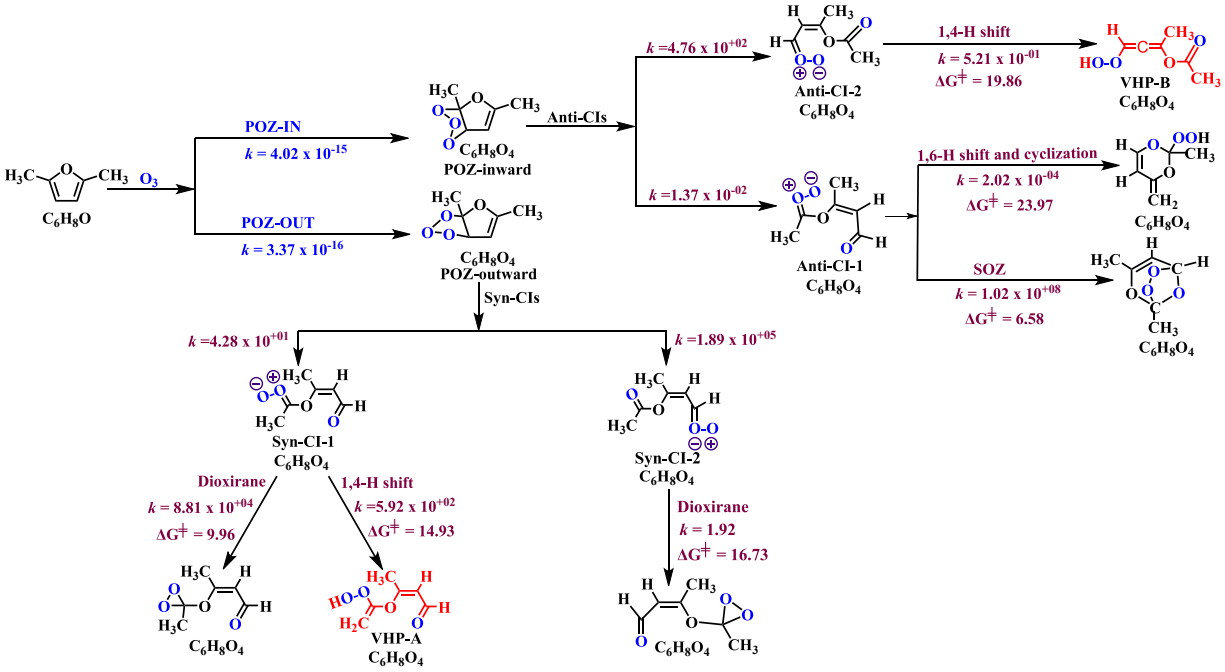


Fig. 6. Ozonolysis of 2,5-DMF showing the formation of two primary ozonides, POZ-IN and POZ-OUT, followed by their decomposition into Anti-CI-1 and Anti-CI-2, and Syn-CI-1 and Syn-CI-2, respectively. The subsequent unimolecular reaction pathways include dioxirane formation and a 1,4-H shift for Syn-CI-1; SOZ formation and a concerted 1,6-H shift with cyclization for Anti-CI-1; dioxirane formation for Syn-CI-2; and a 1,4-H shift for Anti-CI-2. Rate coefficients (k, s^{-1} for unimolecular reactions and cm^3 $molecule^{-1}$ s^{-1} for bimolecular reactions) and barrier heights ($\Delta G^{\ddagger}$, kcal mol^{-1}) were calculated at the RHF-RCCSD(T)-F12a/VDZ-F12//M06-2X/aug-cc-pVTZ level of theory. Colour code: purple indicates unimolecular rate coefficients and activation barriers, while blue indicates bimolecular rate coefficients. Red highlights intermediates that undergo subsequent reaction steps leading toward HOM formation, while blue oxygen atoms indicate those originating from O_3.

Comment 6.)

REVIEWER COMMENT

The reaction of 2,5-DMF with ozone has been investigated experimentally in previous studies. The authors specifically refer to a chamber study (Illmann and Rösgen, 2024) in which product formation was monitored by FTIR and PTR-MS, resulting in a carbon balance below 50 %. While I agree with the authors that this low carbon balance might be due to the inability of these techniques to detect higher oxygenated species, I am wondering whether the authors could provide any quantitative information, such as an estimate of the HOM yield? The authors state that "these low-volatility products [...] may contribute to the >50% carbon balance deficit". I think it would be useful, if possible, to provide the reader with an estimate of the magnitude of the formation of low-volatility products. I would have assumed that a HOM yield should be well below the 50 % deficit, particularly since one of the key routes to HOM formation identified by the authors involves a CI conformer whose branching fraction appears to be rather low. Could the authors comment on this and, if possible, provide a quantitative estimate of the contribution of HOM formation?

RESPONSE

We thank the reviewer for the suggestion. We can now provide a quantitative estimate. Sulfuric-acid calibration of the instrument, following the method of Kürten et al. (2012), gives a calibration coefficient of 8.24×10^9 molecules cm^{-3} per ncps. As is standard practice for HOMs (species carrying six or more oxygen atoms), we assume their ion-molecule reaction with NO_3^- proceeds at the same rate as for sulfuric acid, and apply this single coefficient to every assigned product. The HOM concentrations are obtained directly from the measured signals and this calibration coefficient; no explicit correction for flow-tube wall loss has been applied. Combining the resulting concentrations with the reacted-precursor amount (Δ[2,5-DMF]) from our Kinetiscope simulation of the reference condition (169 ppbv 2,5-DMF, 54 ppbv O_3, 21 ppbv TME, $\Delta t = 7\,s$) gives a yield $Y_{HOM} = \Delta HOM/\Delta VOC$. Summing the assigned RO_2 radicals, closed-shell termination products, accretion products, and fragmentation products (the RO_2/ROOH/Accretion/Fragment rows of Table 2) gives $Y_{HOM} \approx 0.85\,\%$ at the 169 ppbv reference condition, and 0.06–1.26 % across the 17–424 ppbv concentration series (Sect. S5, Fig. S6, Table S1). This is well below the reviewer's >50 % carbon balance deficit, as expected given the very low assumed population of the specific reactive Criegee intermediate (Anti-CI-2A, ~0.01 % of the inward-POZ-derived population) invoked for the O_9-forming pathway – distinct from the dominant Anti-CI-2 conformer itself (89.48 %). HOM formation therefore accounts for only a small part of the missing carbon. Because the estimate rests on one fixed sensitivity applied across all products, and wall losses are not corrected for, we treat these values as order-of-magnitude estimates with an asymmetric, roughly factor-of-two uncertainty ($-50\,\%/+100\,\%$), and the Atmospheric Implications section accordingly states a HOM yield of order 0.1–1 % rather than a single value.

CHANGES TO MANUSCRIPT

Atmospheric Implications section, lines 533–535 ("...Under the 169 ppbv 2,5-DMF + O_3 + TME condition (Fig. 3b), we estimate a HOM yield of order 0.1–1 % (see Sects. S5 and S6 of the Supplement) – a low molar yield, but one that, as in other autoxidation systems, can still drive disproportionate SOA growth and new particle formation (Wang et al., 2021)."): replaced "A quantitative HOM yield cannot be derived from the present data set..." with the quoted sentence above.

CHANGES TO SUPPLEMENT

Sect. S5, lines 49–68, Fig. S6, Table S1, and Sect. S6.1: new Sect. S5 ("HOM yield as a function of 2,5-DMF concentration"): added the full quantitative derivation – a sulfuric-acid-derived NO_3^- CIMS calibration coefficient ($C = 8.24 \times 10^9$ molecules cm^{-3} per ncps, following Kürten et al. (2012)) applied uniformly to all assigned products, summing the RO_2/ROOH/accretion/fragment species and combined with the reacted-precursor concentration from kinetic simulation, giving $Y_{\mathrm{HOM}} \approx 0.85\,\%$ at the 169 ppbv reference condition and increasing monotonically from about 0.06 % at 17 ppbv to about 1.26 % at 424 ppbv across the full concentration series (new Fig. S6; new Table S1), reported with an asymmetric, roughly factor-of-two uncertainty ($-50\,\%/+100\,\%$). The new Sect. S5 text reads: "To probe how strongly the HOM yield depends on precursor loading, we recorded a 2,5-DMF concentration series (17–424 ppbv) at fixed [O_3] = 54 ppbv and [TME] = 21 ppbv, $\Delta t = 7$ s. [...] At the 169 ppbv reference condition, this treatment gives $Y_{\mathrm{HOM}} \approx 0.85\,\%$, and across the full series the yield is seen to increase monotonically with precursor loading, from about 0.06 % at 17 ppbv to about 1.26 % at 424 ppbv (Fig. S6; Table S1)." The calibration, assumptions, and uncertainty are described in Sect. S5, lines 49–68; consumed precursor is defined in Sect. S6.1. Addition to Supplement: the yield figure and table are reproduced below.

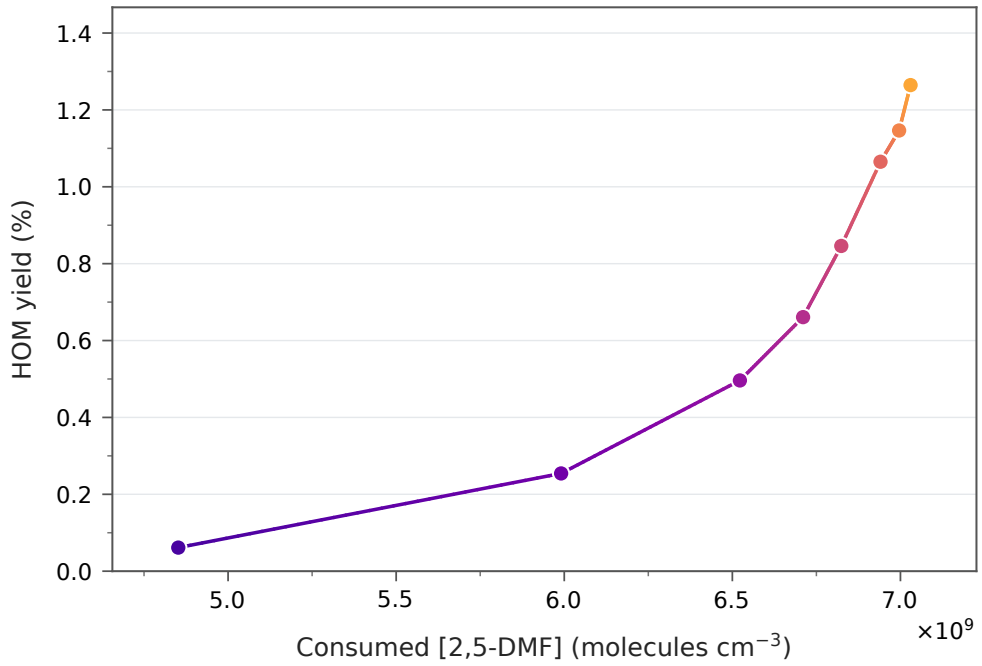


Fig. S6. HOM yield (Y_{HOM}, Eq. S1; Table S1) as a function of consumed 2,5-DMF concentration, for the 2,5-DMF concentration series at fixed [O_3] = 54 ppbv and [TME] = 21 ppbv, $\Delta t = 7$ s. Marker and connecting-line color encodes the consumed [2,5-DMF] concentration (sequential colormap, low to high) purely to aid visual tracking between adjacent points along the x-axis; it does not represent an independent variable.

Table S1. HOM yield (Y_{HOM}) as a function of 2,5-DMF concentration, at fixed [O_3] = 54 ppbv and [TME] = 21 ppbv, $\Delta t = 7$ s. Δ[2,5-DMF] is the consumed-precursor concentration obtained from the kinetic simulation (Sect. S6.1). Y_{HOM} sums the assigned RO_2 radicals, closed-shell termination products, accretion products, and the five O_6/O_7 fragmentation products.

[2,5-DMF] (ppbv)	**Δ[2,5-DMF]** (10^9 molecules cm^{-3})	Y_{HOM} (%)
17	4.85	0.061
42	5.99	0.254
85	6.52	0.496
127	6.71	0.661
169	6.82	0.846
254	6.94	1.065
339	7.00	1.146
424	7.03	1.265

Specific comments

REVIEWER COMMENT

Table 1: "concentration (ppb)" should be "mixing ratio (ppb)"

RESPONSE

Corrected as suggested.

CHANGES TO MANUSCRIPT

Methods section, Table 1 (manuscript p. 6, Table 1 is placed between lines 118 and 119): column heading changed from "Reactant concentration (ppb)" to "Reactant mixing ratio (ppb)".

REVIEWER COMMENT

Lines 192-194: I would encourage the authors to rephrase this sentence, since the peroxy radicals differ not only in the number of hydrogen atoms, but also in the number of oxygen atoms. Perhaps it would be clearer to say that the oxidant channels produce structurally distinct RO_2 radicals, resulting in two separable product families that differ by two hydrogen atoms?

RESPONSE

We thank the reviewer for this suggestion and have adopted the proposed phrasing. The original sentence stated that the RO_2 radicals themselves differ by two hydrogen atoms, but, as the reviewer notes, the two channels' radicals also differ in oxygen content, so that description was incomplete. The two families differ by two hydrogen atoms, with either different or the same oxygen content: the OH-initiated chain proceeds through even-oxygen radicals ($C_6H_9O_4 \rightarrow O_6 \rightarrow O_8$), whereas the dominant ozonolysis-initiated chain proceeds through odd-oxygen radicals ($C_6H_7O_5 \rightarrow O_7 \rightarrow O_9$). The revised sentence therefore describes the channels as producing structurally distinct RO_2 radicals that differ in oxygen content, and attributes the two-hydrogen offset to the resulting product families, where it strictly applies.

CHANGES TO MANUSCRIPT

Results section, lines 211–213: Sect. 3.1, opening paragraph, now reads: "The two oxidant channels, OH and

O_3, produce structurally distinct RO_2 radicals, differing in oxygen content (predominantly an even number of O atoms for the OH-derived $C_6H_9O_x$ and an odd number for the O_3-derived $C_6H_7O_x$ radicals), resulting in two separable product families that differ by two hydrogen atoms, detectable by NO_3^- CIMS (Fig. 1)."

REVIEWER COMMENT

Lines 229-231: The sentence starting with "The C_{10} composition" is somewhat difficult to follow. I would encourage the authors to reformulate it for clarity.

RESPONSE

We thank the reviewer for the comment. We have reformulated this sentence to spell out the fragment-combination logic explicitly rather than leaving the reader to infer it: we now name both candidate carbon pairings (C_4+C_6 and C_5+C_5) of peroxy radicals that are consistent with the observed composition.

CHANGES TO MANUSCRIPT

Results section, lines 258–260: Results section: "The C_{10} compositions ($C_{10}H_{12}O_8$ and $C_{10}H_{14}O_6$–9) contain two fewer carbon atoms than the C_{12} expected from two intact C_6 peroxy radicals. This is consistent with either accretion of a C_4 peroxy radical with an intact C_6 partner, or of two C_5 peroxy radicals with each other."

REVIEWER COMMENT

Lines 246-248: I do not entirely understand this sentence. What do the authors mean by a competition between recombination and fragmentation pathways? I would have assumed that both arise from bimolecular reactions, in which case their relative contributions should not depend on the RO_2 concentration. Could the authors please rephrase this statement or provide some additional information to clarify what is meant here?

RESPONSE

We agree: recombination and fragmentation are both unimolecular decay channels of the same RO···OR' complex, so their relative branching does not itself depend on RO_2 concentration, and only the rate at which such complexes form in the first place does, since that step is bimolecular. We have removed the competition framing and reworded the sentence to describe only this bimolecular step: the $C_{12}H_{18}O_8$ accretion product appears exclusively under TME conditions because the higher RO_2 concentrations generated by the added OH source increase the rate of RO_2+RO_2 encounters, giving a higher yield of the RO···OR' complex available to recombine.

CHANGES TO MANUSCRIPT

Results section, lines 275–277: Results section, TME discussion: "Its appearance exclusively under TME conditions reflects the higher RO_2 concentrations generated by the added OH source, which increase the rate of bimolecular RO_2+RO_2 encounters and thereby the yield of the RO···OR' complex available to recombine."

REVIEWER COMMENT

Line 314: "Fig ??" should be "Fig 8"?

RESPONSE

This is the same cross-reference correction as in our response to Referee #1 (pp. 17 and 22); it now resolves correctly to Fig. 8a.

CHANGES TO MANUSCRIPT

Results section, Sect. 3.4.2, line 400 (previously ‘Fig. ??’): “...as shown in Fig. 8 a.”